Geological Society of America
Special Paper 403
2006

Petrologic characterization of Guatemalan lawsonite eclogite: Eclogitization of subducted oceanic crust in a cold subduction zone

Tatsuki Tsujimori*
Department of Geological and Environmental Sciences, Stanford University, Stanford, California 94305-2115, USA
Virginia B. Sisson
Department of Earth and Planetary Sciences, American Museum of Natural History, New York, New York 10024-5192, USA
Juhn G. Liou
Department of Geological and Environmental Sciences, Stanford University, Stanford, California 94305-2115, USA
George E. Harlow
Department of Earth and Planetary Sciences, American Museum of Natural History, New York, New York 10024-5192, USA
Sorena S. Sorensen
Department of Mineral Sciences, National Museum of Natural History, Smithsonian Institution, Washington, D.C. 20560-0119, USA

ABSTRACT

Early Cretaceous lawsonite eclogites and related high-pressure rocks occur as tectonic inclusions within serpentinite mélange south of the Motagua fault zone, Guatemala. Petrologic and microtextural analyses of mafic high-pressure rocks reveal three metamorphic stages linked to several deformational textures. The prograde stage represents an incipient eclogitization and is preserved in prograde garnet, along with an older S_1–S_2 foliation. The prograde assemblage is garnet (X_{Mg} = ~0.22) + omphacite (~52 mol% jadeite) or jadeite (~83 mol % jadeite) + lawsonite + chlorite + rutile + quartz ± phengite (3.6 Si p.f.u.); some rocks also have ilmenite and rare ferro-glaucophane. Lawsonite in garnet of some lawsonite eclogites contains rare pumpellyite inclusions. The presence of synmetamorphic brittle deformation, inclusions of pumpellyite, Fe^{2+}-Mg distribution coefficients between omphacite inclusions and adjacent garnet with Ln(K_D) = 2.7–4.5, and garnet-clinopyroxene-phengite thermobarometry suggest that eclogitization initiated at temperature (*T*) = ~300 °C and pressure (*P*) > 1.1 GPa, and continued to *T* = ~480 °C and *P* = ~2.6 GPa. In contrast, the retrograde eclogite-facies assemblage is characterized by reversely zoned garnet rims and omphacite ± glaucophane + lawsonite + rutile + quartz ± phengite (3.5 Si p.f.u.) along the S_3 foliation. Garnet-phengite-clinopyroxene thermobarometry yields *P* = ~1.8 GPa and *T* = ~400 °C. The youngest, blueschist-facies assemblage (glaucophane + lawsonite + chlorite + titanite + quartz ± phengite) locally replaces earlier mineral assemblages along S_4 crenulations. The inferred prograde *P-T* trajectory lies near a geotherm of ~5 °C km^{-1}, comparable to the calculated thermal and petrologic structure of the NE Japan subduction zone. These petrologic characteristics indicate:

*tatsukix@pangea.stanford.edu.

Tsujimori, T., Sisson, V.B., Liou, J.G., Harlow, G.E., and Sorensen, S.S., 2006, Petrologic characterization of Guatemalan lawsonite eclogite: Eclogitization of subducted oceanic crust in a cold subduction zone, *in* Hacker, B.R., McClelland, W.C., and Liou, J.G., eds., Ultrahigh-pressure metamorphism: Deep continental subduction: Geological Society of America Special Paper 403, p. 147–168, doi: 10.1130/2006.2403(09). For permission to copy, contact editing@geosociety.org.

(1) the basalt-eclogite transformation may occur at *T* = ~300 °C in cold subduction zones, (2) glaucophane-bearing prograde assemblages are rare during incipient eclogitization in cold subduction zones, and (3) the chlorite-consuming reactions that form Fe-Mg-Mn garnet are more effective than the lawsonite-consuming reaction that forms a grossular component. At depths of ~100 km in cold subduction zones, dehydration embrittlement may be caused by such chlorite-consuming reactions.

Keywords: cold subduction, HP-UHP metamorphism, lawsonite eclogite, P-T trajectory, Guatemala.

INTRODUCTION

An incredibly cool paleogeotherm near ~5 °C km^{-1} is one of the critical features of diamond-bearing ultrahigh-pressure (UHP) metamorphic rocks as well as lawsonite eclogites (e.g., Liou et al., 2000; Rumble et al., 2003; Maruyama and Liou, 2005). Although preservation of such an extremely low geotherm is rare in orogenic belts, thermal models of subduction zones predict cold temperatures in subduction zones where old lithosphere is rapidly subducting, such as beneath present-day Tonga and NE Japan (e.g., Kirby et al., 1996; Peacock and Wang, 1999; Peacock, 2001; Hacker et al., 2003a, 2003b). Also, experiments using mid-ocean-ridge basalt (MORB) compositions as precursors predict that subducted oceanic crust transforms to lawsonite eclogite from blueschist (e.g., Pawley, 1994; Poli and Schmidt, 1995; Pawley et al., 1996; Okamoto and Maruyama, 1999). Furthermore, lawsonite is stable along a cold geotherm down to 300 km depth and is proposed to be a major H_2O reservoir in subducted oceanic crust. The occurrence of lawsonite eclogite xenoliths in ultramafic diatremes of the Colorado Plateau (Watson and Morton, 1969; Helmstaedt and Schulze, 1988; Usui et al., 2003) implies that lawsonite-eclogite–facies conditions may be common in Pacific-type subduction. Questions about this process include: how does downgoing oceanic crust transform to lawsonite eclogite in a cold subduction? What are the pressure-temperature (*P-T*) paths for lawsonite eclogites? What prograde dehydration events are preserved in lawsonite eclogites during eclogitization?

So far, at least ten localities of lawsonite eclogite are known (excluding xenoliths), including (1) Motagua fault zone, Guatemala (McBirney et al., 1967; Smith and Gendron, 1997; Harlow et al., 2003, 2004; Tsujimori et al., 2005), (2) Samaná Peninsula, Hispaniola (Dominican Republic) (Zack et al., 2004), (3) Schistes Lustrés, Corsica (Caron et al., 1981; Caron and Péquignot, 1986), (4) Central Pontides, Turkey (Altherr et al., 2004), (5) Port Macquarie, New England fold belt, Australia (Och et al., 2003), (6) Pinchi Lake, British Columbia, Canada (Ghent et al., 1993), (7) Ward Creek, Franciscan complex, California, USA (Maruyama and Liou, 1988; Oh et al., 1991; Shibakusa and Maekawa, 1997), (8) Barru complex, Sulawesi, Indonesia (Parkinson et al., 1998), (9) Pam Peninsula, New Caledonia (Clarke et al., 1997), and (10) Motalafjella, western Spitsbergen (Hirajima et al., 1988) (See review of Tsujimori et al., 2006). Elsewhere higher-*T* epidote-bearing assemblages variably overprint most lawsonite-eclogite assemblages. In contrast, the Guatemalan lawsonite eclogite contains garnet porphyroblasts that grew only within the lawsonite stability field (Tsujimori et al., 2005). In this paper, we describe the detailed petrologic characteristics of the Guatemalan lawsonite eclogite. Together with microstructural features, these data are used to establish the prograde and retrograde *P-T* paths. This characterization of lawsonite eclogite helps us to understand metamorphic processes in a cold subduction zone with an extremely low geotherm.

Mineral abbreviations are after Kretz (1983); we also use aegirine (Ae), ferroglaucophane (Fgl), phengite (Phe), and coesite (Coe) throughout this paper.

GEOLOGIC SETTING

Active volcanic arcs or strike-slip fault systems characterize the present-day Caribbean plate margins. Along the northern and southern plate margins, there are Cretaceous blueschists, and eclogites (±rare garnet peridotites) extending from Guatemala (e.g., Tsujimori et al., 2005), through Cuba (e.g., Schneider et al. 2004), Jamaica (Draper, 1986), and Dominican Republic (e.g., Giaramita and Sorensen, 1994; Abbott et al., 2005) and farther south to Venezuela (e.g., Sisson et al., 1997) and Colombia (Green et al., 1968) (Fig. 1). These high-pressure rocks are associated with serpentinite, Jurassic-Cretaceous ophiolites, and/or accretionary complexes. The protoliths for these various high-pressure terranes vary from MORB to continental lithologies to island-arc volcanics (e.g., Sorensen et al., 1997, 2005; Beccaluva et al., 1995; Unger et al., 2005).

The northern boundary of the Caribbean plate in Guatemala is the Motagua fault zone, a left-lateral strike-slip fault that is part of the suture zone juxtaposing the Maya and Chortís continental blocks. The Motagua fault zone extends into the Caribbean plate along the Swan Islands fracture zone to the Cayman Trough. Along the Motagua fault zone in central Guatemala, serpentinite bodies are exposed on either side of the Río Motagua; the serpentinite-matrix mélange stretches ~220 km throughout central and eastern Guatemala (e.g., Harlow et al., 2004) (Fig. 2). The strike-slip fault system includes the E-W–trending Sierra de Chuacús and Sierra de Las Minas. To the north, the Motagua fault zone is bounded by epidote-amphibolite– to amphibolite-facies gneiss and schist with rare relict eclogites of the Chuacús

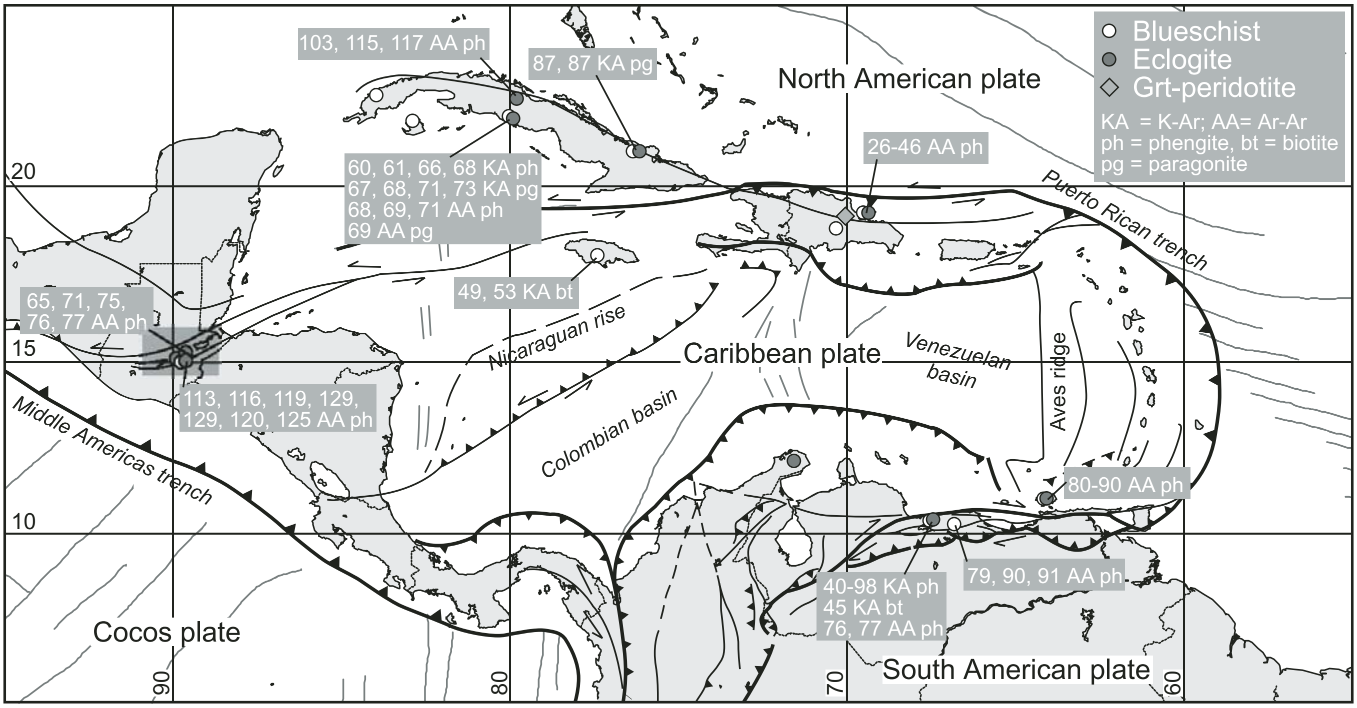

Figure 1. Tectonic framework of the Caribbean region showing representative localities of Cretaceous high-pressure–ultrahigh-pressure (UHP) rocks. Phengite and paragonite K-Ar and Ar-Ar ages are from Somin et al. (1992), Stöckhert et al. (1995), Smith et al. (1999), Gonçalves et al. (2000), Schneider et al. (2004), and Harlow et al. (2004).

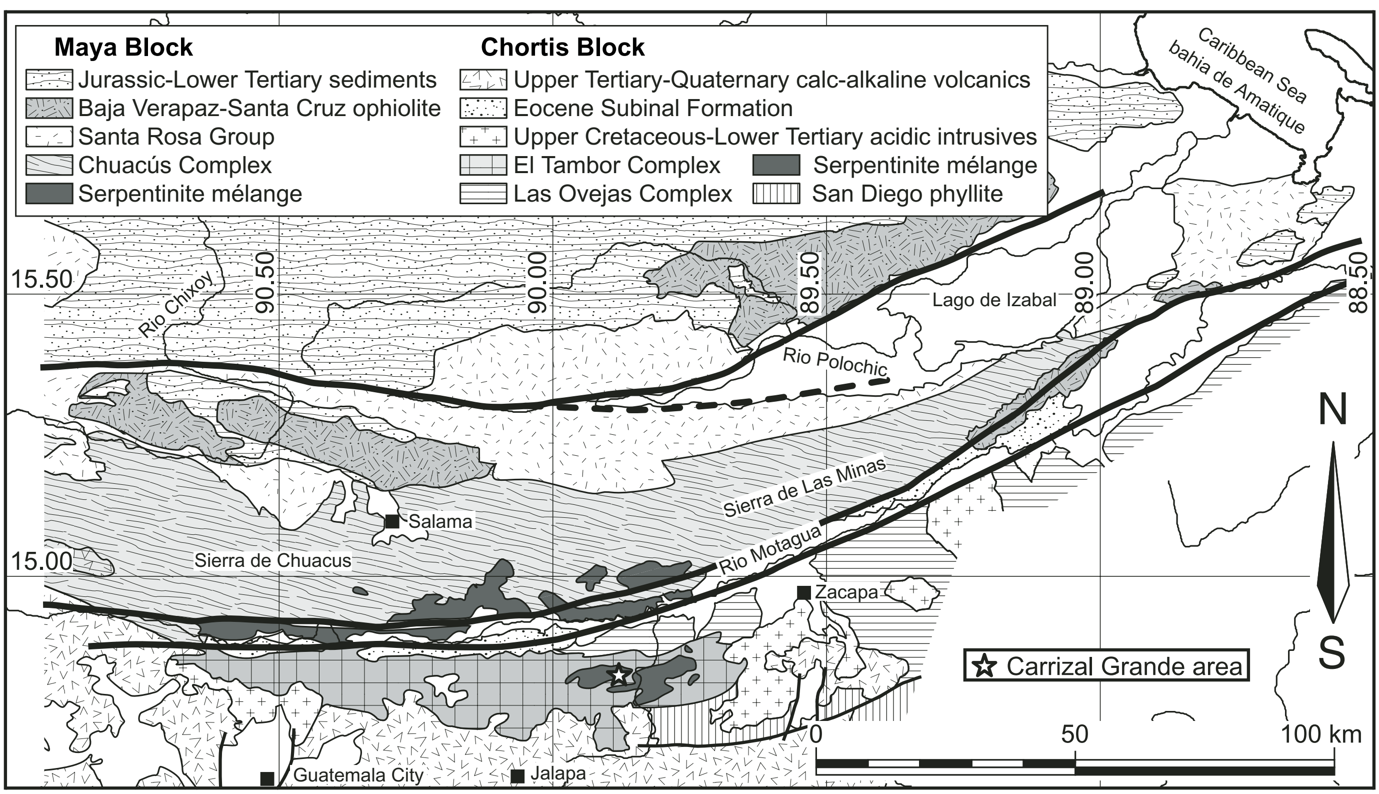

Figure 2. Simplified geologic map of central Guatemala, showing eclogite localities (modified after Beccaluva et al., 1995).

terrane (Ortega-Gutiérrez et al., 2004). North of the Chuacús terrane, Paleozoic Santa Rosa Group sediment and deformed granite constitute the basement of the Maya block. To the south, the basement of the Chortís block is the low-grade greenschist-facies San Diego phyllite and amphibolite-facies Las Ovejas complex.

The serpentinite-matrix mélange along the Motagua fault zone consists of meter-size blocks of ophiolitic rocks, high-pressure metamorphic rocks, and various metasomatic rocks. Some of the serpentinites host world-class localities of jadeitite (e.g., Harlow, 1994). Based on dissimilar rock assemblages and $^{40}Ar/^{39}Ar$ phengite geochronology, the serpentinite-matrix mélange can be divided into northern and southern belts (Harlow et al., 2004). The northern belt consists of amphibolite, gneiss, amphibolitized epidote-eclogite, and jadeitite with phengite $^{40}Ar/^{39}Ar$ integrated ages of 77–65 Ma. In contrast, the southern belt is characterized by blueschist, lawsonite eclogite, and lawsonite-bearing jadeite with phengite $^{40}Ar/^{39}Ar$ integrated ages of 125–116 Ma. The southern eclogite has an Sm-Nd garnet–omphacite–whole-rock isochron age of 135 Ma (Sisson et al., 2003). These Cretaceous cooling ages are mostly comparable to those of eclogites and blueschists from Cuba, Hispaniola, and Venezuela (e.g., Somin et al., 1992; Gonçalves et al., 2000; Schneider et al., 2004; Sisson et al., 2005).

ECLOGITES IN THE QUEBRADA DEL MICO AND QUEBRADA SECA

Mode of Occurrence

A fault-bounded eclogite-bearing serpentinite mélange unit occurs in the Carrizal Grande area, south of the Motagua fault zone (Fig. 2). A large amount of eclogite and related rocks are exposed as loose blocks (<10 m) in landslide debris along the Quebrada El Silencio, Quebrada del Mico, and the Quebrada Seca, streams that feed into Río Jalapa or El Tambor. The eclogitic blocks are sandwiched between antigorite serpentinite and phyllite, and the exposures cover an area of ~4 × 0.5 km. The blocks include eclogitic rocks, minor jadeitite, and mica schist (phengite-rich schist); rare eclogites intercalated with graphite-bearing quartz mica schists suggest a protolith mixture of mafic rocks with some semipelagic sedimentary rocks. Serpentinite associated with eclogitic blocks consist of schistose, friable antigorite serpentinite. The eclogitic blocks are rounded; rare tremolite- or glaucophane-rich rinds are observed. At least four types of eclogitic rocks are recognized: jadeite-bearing lawsonite eclogite, type I lawsonite eclogite, type II lawsonite eclogite, and garnet-bearing lawsonite blueschist (Fig. 3). The jadeite-bearing lawsonite eclogite is a pale-green, weakly foliated, rare rock containing up to 75 vol% garnet + clinopyroxene; it can be subdivided into fine- and coarse-grained varieties based on the size of the garnet porphyroblasts. In particular, the coarse-grained jadeite-bearing lawsonite eclogite has garnet porphyroblasts up to 1.5–2.5 cm in diameter (Tsujimori et al., 2005) (Fig. 3A). Type I lawsonite eclogite, dominant in Quebrada del Mico, is green and massive, with 0.5–1.0 cm garnet (Fig. 3B). Type I lawsonite eclogite is cut by irregularly shaped, retrograde, glaucophane-rich hydrous veins (1–15 cm wide). Type II lawsonite eclogite is well-foliated glaucophane-bearing eclogite (Fig. 3C), and the dominant rock in Quebrada Seca. Most have millimeter- to centimeter-scale compositional banding defined by omphacite- and glaucophane-bearing layers. The modal abundance of garnet + omphacite reaches locally up to 80% in type I and II lawsonite eclogite. Garnet-bearing lawsonite blueschist is a well-foliated schist that contains omphacite (<10 vol%) (Fig. 3D).

Textural Variation and Structural Framework

Most eclogitic rocks in the Carrizal Grande area preserve textural evidence for multiple stages of deformation, prograde metamorphism, and retrograde metamorphism prior to the formation of the mélange (Fig. 3). Similar deformation relationships in various blocks enable us to explain their synmetamorphic deformational history.

Meso- and microstructural analyses show four phases of deformations: D_1, D_2, D_3, and D_4 (Fig. 4), based on overprinting relationships among polyphase tight-isoclinal folds, boudinaged layers, inclusion trails in garnet, and late crenulations. The D_3 phase of deformation and recrystallization is dominant in most rocks. In particular, penetrative S_3 schistosity can be observed in all type II lawsonite eclogite and garnet-bearing quartz–phengite schist (Figs. 3C, 4E, and 4I). The early S_2 schistosity is preserved in jadeite-bearing lawsonite eclogite, type I lawsonite eclogite, and rare type II lawsonite eclogite (Fig. 3A). The transition from S_2 to S_3 is observed in F_3 folds; S_2 was folded during D_3 with the development of newly formed S_3 along the axial planes of F_3 folds (Figs. 3H and 3I). The schistosity in garnet-bearing quartz–phengite schist is presumed equivalent to S_3, and inclusion trails in garnet that are nearly perpendicular to matrix schistosity may be equivalent to S_2 (Fig. 3E). During D_3, type I lawsonite eclogite was boudinaged within its glaucophane-rich host type II lawsonite eclogite (Fig. 3D). Jadeite-bearing lawsonite eclogite that preserves pre-D_3 structures is interpreted as meter-scale boudins barely affected by D_3. Evidence of D_1 includes S_1 inclusion trails in garnet of jadeite-bearing lawsonite eclogite (Fig. 3A); inclusion trails comparable to S_1 are rarely observed in garnet cores in garnet-bearing quartz–phengite schist (see later section). D_4 deformation is minor, but includes open F_4 crenulations in garnet-bearing lawsonite blueschist (Fig. 3D). Centimeter-scale chevron folds in a loose block of serpentinite may be part of D_4 (Fig. 3F). Note, these stages of deformation are mostly within the eclogite blocks and are different from the five generations of ductile and four stages of brittle deformation observed in the basement and host serpentinite (e.g., Francis et al., 2005; Francis, 2005). For example, chevron folds in serpentinite can also be related to chevron folds formed during the D_5 deformation seen in the San Diego phyllite (Francis, 2005).

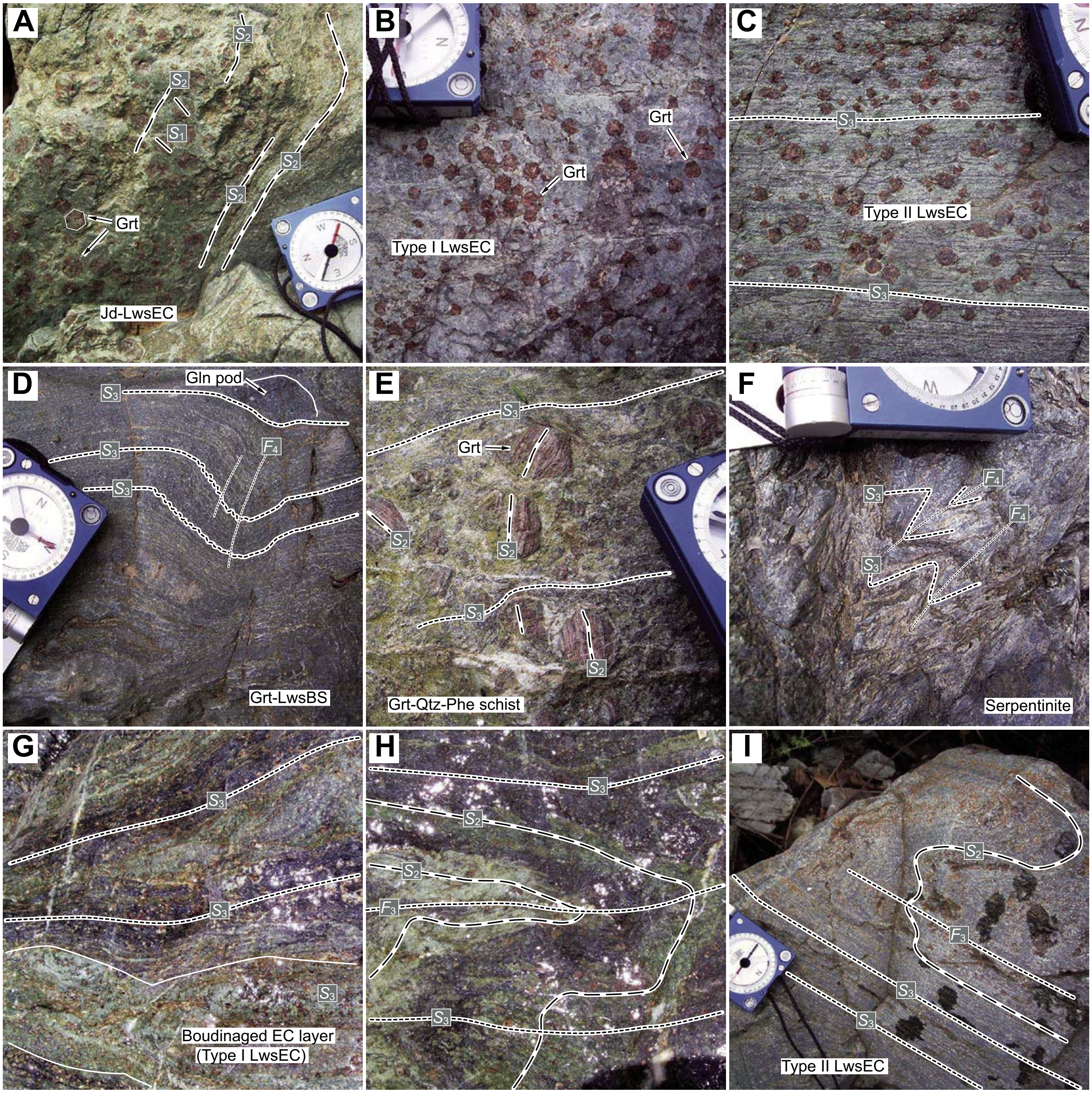

Figure 3. Representative structures of the Carrizal Grande high-pressure rocks. Geologic compass (7 cm wide) is for scale. (A) Coarse-grained jadeite-bearing lawsonite eclogite (Jd-LwsEc) containing large euhedral garnets (Grt) up to 2.5 cm. S_1 inclusion trails in garnet are nearly perpendicular to matrix schistosity S_2. (B) Type I lawsonite eclogite containing euhedral garnets. (C) Type II lawsonite eclogite showing a penetrative S_3 schistosity. (D) Garnet-bearing lawsonite blueschist (Grt-LwsBS) showing D_4 deformation and glaucophane (Gln) pod. (E) Coarse-grained garnet-bearing quartz–phengite (Grt-Qtz-Phe) schist containing garnets up to 2.5 cm. (F) Schistose antigorite serpentinite with chevron folds. (G) Boudinaged type I lawsonite eclogite layer. Field of view is about 20 cm. (H) Isoclinal fold of partially hydrated type I lawsonite eclogite showing the transition from S_2 to S_3; S_2 was folded during D_3 with the development of S_3 along the F_3 axial planes. Field of view is about 30 cm. (I) Isoclinal folds in type II lawsonite eclogite showing the transition from S_2 to S_3.

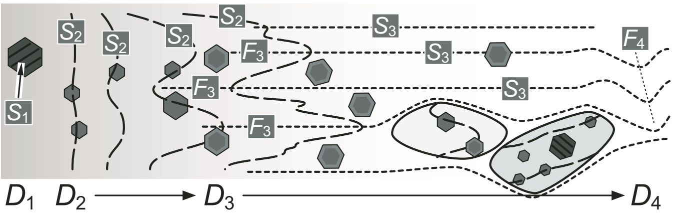

Figure 4. Schematic illustration showing development of the structural relationships.

PETROGRAPHY

Jadeite-Bearing Lawsonite Eclogites

The jadeite-bearing lawsonite eclogites are subdivided into coarse- and fine-grained rocks. The coarse-grained jadeite-bearing lawsonite eclogites have two generations of jadeitic pyroxene, which consist of sodic pyroxene and garnet, with minor rutile, phengite, chlorite, ferroglaucophane, lawsonite, titanite, ilmenite, and quartz (Tsujimori et al., 2005). Large garnet porphyroblasts (1.5–2.5 cm) contain oriented inclusions of sodic pyroxene, rutile, ferroglaucophane, quartz, lawsonite, and phengite with inclusions of chlorite and ilmenite are restricted to garnet cores. Inclusion trails in garnet define an internal S_1 foliation. The weakly foliated matrix consists of sodic pyroxene with minor lawsonite, rutile, quartz, and phengite; the preferred orientation of phengite and fine-grained sodic pyroxene define an S_2 foliation at a high angle to the internal fabric S_1 in garnet. Impure first-generation jadeite (Jd-I) occurs as subhedral blasts up to 1.5 mm in length, while second generation jadeitic pyroxene (Jd-II) occurs in fine-grained aggregates associated with minor omphacite (Fig. 5A). Matrix rutile is often rimmed by titanite; rare matrix jadeitic pyroxene may be replaced by albite. Although the effects of D_3 and D_4 were not recognized, the matrix was partly recrystallized during retrogression.

The fine-grained lawsonite eclogite lacks the centimeter-size large garnet (Fig. 5B); garnet porphyroblasts, up to 4 mm in size, are scattered in a nematoblastic foliation S_2 defined by preferred orientation of prismatic omphacite (<1 mm in length) and phengite. It contains omphacite and garnet with minor amounts of lawsonite, jadeite, phengite, quartz, and rutile. Rare albite is found as a secondary mineral replacing jadeite. Subhedral garnet contains mineral inclusions of omphacite, phengite, rutile, and tiny (<0.05 mm) lawsonite and rare quartz; inclusion trails are in continuity with external foliation S_2. Another important feature is that the older inclusion trail S_1 is not present. In some samples, matrix omphacite is partially contained within garnet. Omphacite is optically zoned, and contains oriented tiny mineral inclusions (<0.02 mm) of quartz and lawsonite in the greenish cores (Fig. 5B). Jadeite occurs as discrete grains (<0.5 mm) and contains rare rutile inclusions. Matrix rutile does not have a titanite rim.

Type I Lawsonite Eclogites

Type I lawsonite eclogite has 5–10 mm euhedral garnet scattered in a fine-grained, granoblastic, weakly foliated matrix (Figs. 5C and 5D). The matrix consists of omphacite and lawsonite, with minor chlorite, titanite, phengite and quartz; locally, omphacite occurs as fine-grained aggregates. Garnet porphyroblasts contain abundant inclusions of lawsonite, omphacite, rutile, ilmenite, and chlorite; most lack ilmenite and chlorite in their rims. Lawsonite inclusions in garnet cores contain rare <0.02 mm pumpellyite. Rutile in garnet does not have a titanite rim. In some samples, nearly inclusion-free garnet rims enclose inclusion-rich garnet. Late-stage phengite occurs along garnet grain boundaries and fills some fractures in garnet. Two different schistosities, S_2 and S_3, are recognized in the matrix. Lawsonite-rich seams and laminae define S_2; also, titanite overgrowths around rutile are aligned parallel to S_2. The S_2 is weakly crenulated, and locally cut by S_3 (Fig. 5D). In some samples, inclusions within garnet show a strong fabric comparable to S_2 that is not continuous with S_3 (Figs. 5D and 5E). These textures indicate that the main growth of garnet occurred during D_2. Crack-seal veins of elongate-blocky omphacite and lawsonite locally break up the matrix (Fig. 5C); these crack-seal veins can be traced into euhedral garnet as bands of oriented coarser omphacite and lawsonite (Fig. 5C). These textures indicate that D_2 involved brittle deformation during eclogite-facies conditions.

In the retrograde glaucophane-rich hydrous veins, the matrix is intensely recrystallized into fine-grained aggregates of glaucophane and omphacite (<0.3 mm) and unoriented, poikiloblastic subhedral to euhedral titanite (<1.5 mm in length). Glaucophane is intergrown with recrystallized omphacite, and titanite contains abundant tiny inclusions of glaucophane and omphacite. Rare coarse-grained phengite also grew in the hydrous veins.

Type II Lawsonite Eclogites

The type II lawsonite eclogite is a glaucophane-bearing nematoblastic matrix containing subhedral to euhedral 3–10 mm garnet, and is composed of omphacite, glaucophane, garnet, and lawsonite, with minor titanite, phengite, chlorite, and quartz. A penetrative S_3 schistosity is defined by oriented prismatic omphacite and glaucophane with granoblastic lawsonite (Figs. 3C and 5G). Garnet porphyroblasts contain inclusions of omphacite, lawsonite, rutile, quartz, and rare phengite. Some garnet cores contain rare K-feldspar—rather than phengite—inclusions. The internal fabric of the inclusions in garnet is discontinuous with the external foliation S_3. In some garnets, nearly inclusion-free rims enclose inclusion-rich cores. Some prismatic omphacites (<0.5 mm in length) contain inclusions of needle-like quartz, lawsonite, rutile, with rare glaucophane in the core. Pale violet glaucophane contains inclusions of rutile, lawsonite, omphacite, and rare zircon. Most lawsonite is twinned and contains rare inclusions of rutile. Titanite replaces most rutile (Fig. 5G), except for rutile inclusions in garnet.

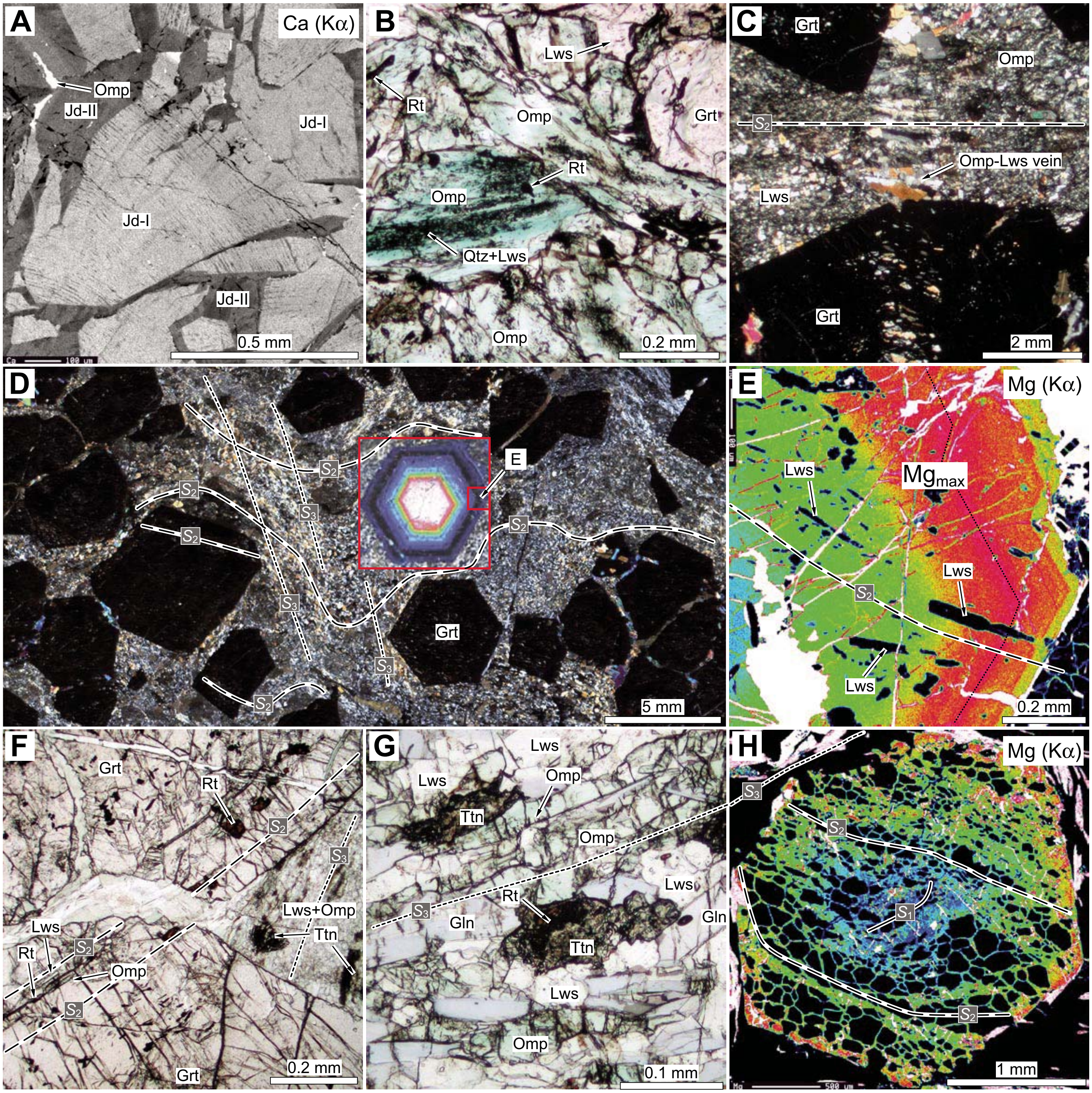

Figure 5. Microtextures of the Carrizal Grande rocks. (A) Backscattered-electron (BSE) image shows two stages of sodic clinopyroxene in the coarse-grained jadeite eclogite. Jd-I is replaced by Jd-II plus minor omphacite (Omp). (B) Photomicrograph in plane polarized light showing inclusion-rich omphacite and garnet in fine-grained jadeite eclogite. Grt—garnet, Lws—lawsonite, Rt—rutile, Qtz—quartz. (C) A synmetamorphic omphacite + lawsonite vein in type I lawsonite eclogite (crossed polarized light). (D) Weakly deformed matrix of type I lawsonite eclogite (crossed polarized light). Image is color X-ray of Mn concentration overlain on a garnet grain. (E) X-ray image of Mg in the rim of the same garnet. (F) Internal inclusion trails within garnets in type I lawsonite eclogite. Ttn—titanite. (G) Glaucophane (Gln)-bearing foliated matrix of type II lawsonite eclogite (plane polarized light). (H) X-ray image of Mg in a garnet showing two internal foliations.

Garnet-Bearing Lawsonite Blueschist

The garnet-bearing lawsonite blueschist is petrographically similar to the type II lawsonite eclogite, but has <10 vol% omphacite. It has a similar mineral assemblage of glaucophane, lawsonite, and garnet with minor omphacite, titanite, phengite, chlorite, and quartz. Garnet porphyroblasts (5–8 mm in size) contain inclusions of omphacite, lawsonite, rutile, quartz, and rare ferroglaucophane. Titanite in the matrix contains rare relict rutile. Recrystallization is more extensive than in the type II lawsonite eclogite. Most garnets have chloritized fractures with rare stilpnomelane. Secondary albite is associated with other retrograde minerals, such as titanite, chlorite and stilpnomelane.

Garnet-Bearing Quartz–Phengite Schist

The garnet-bearing quartz–phengite schist is a lepidoblastic, micaceous metapelite composed of quartz and phengite, minor garnet, lawsonite, glaucophane, rutile, titanite, and graphite. A penetrative S_3 schistosity defined by the preferred orientation of phengite is locally gently folded and crenulated (F_4) (Fig. 3D). Garnet occurs as euhedral to subhedral grains with a bimodal size distribution. Most millimeter-size garnets (normally 0.2–4 mm; rarely up to 2 cm) are poikiloblastic, with inclusions of granoblastic quartz, lawsonite, and fine-grained phengite (Fig. 5H) that preserve an early S_2 schistosity (Figs. 3E and 5H). In contrast, small garnet grains (<0.5 mm) are inclusion free and lie parallel to S_3. Pre-S_2 inclusion trails interpreted as S_1 can be seen in the large garnet cores (Fig. 5H). Lawsonite occurs as poikiloblastic, subhedral prisms (<1.5 mm) containing inclusions of quartz, rutile, garnet, and phengite; rare pumpellyite is included in lawsonite. Nearly colorless, nematoblastic glaucophane is <2 mm wide and contains inclusions of garnet and rutile. Some glaucophane is replaced by fine-grained aggregates of actinolite and chlorite.

MINERAL PARAGENESES AND METAMORPHIC STAGES

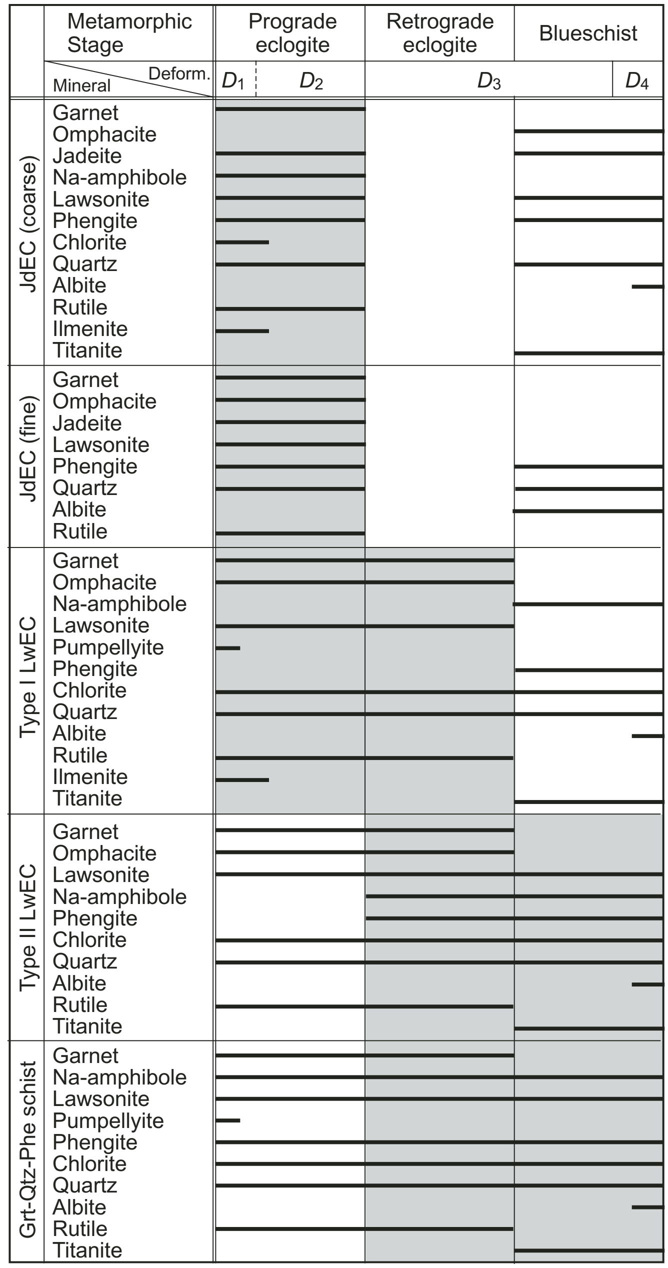

Figure 6. Mineral parageneses for the different stages of metamorphic recrystallization. Grt-Qtz-Phe schist—garnet-bearing quartz–phengite schist; LwEC—lawsonite eclogite; JdEC—jadeite eclogite.

At least two metamorphic stages, an eclogite stage and a blueschist stage, can be distinguished in all rock types. Moreover, the eclogite stage can be subdivided further into prograde eclogite and retrograde eclogite stages. Mineral parageneses for the different metamorphic stages are summarized in Figure 6. The prograde eclogite stage is recorded in prograde-zoned garnet with older S_2 (or S_1) foliation, whereas the retrograde eclogite stage is recorded in reversely zoned narrow garnet rims and in the mineral assemblage formed during S_3. The blueschist stage represents post–eclogite-facies recrystallization and hydration during decompression.

The mineral assemblages and their pseudomorphs formed during S_2 (or S_1) characterize the prograde eclogite stage. This includes Grt + Omp + Lws + Rt + Qtz in mafic lithologies; some rocks also have chlorite, phengite, ferroglaucophane, ilmenite, and K-feldspar. Jadeite occurs instead of omphacite in jadeite eclogite. Eclogite-stage chlorite can be texturally distinguished from later blueschist-stage chlorite. Rare lawsonite contains pumpellyite as precursor inclusions. The minerals of this metamorphic stage are best preserved in the prograde-zoned garnets in all mafic lithologies and in the matrix of the fine-grained jadeite eclogite. The retrograde eclogite stage includes the reversely zoned rims of Grt plus Omp + Lws ± Gln + Rt + Qtz ± Phe ± Chl. This assemblage is best preserved in type II lawsonite eclogite and garnet-bearing lawsonite blueschist. Glaucophane and lawsonite containing rutile or omphacite inclusions are interpreted to be part of this stage. The post–eclogite-stage blueschist-facies overprint that locally replaces earlier mineral assemblages is Gln + Lws + Chl + Phe + Ttn + Qtz (±rare Ab). Titanite overgrowths on rutile and glaucophane-rich hydrous veins are typical features for this stage. In the coarse-grained jadeite eclogite, retrograde jadeite described by Tsujimori et al. (2005) may be part of this stage.

MINERAL CHEMISTRY

Electron microprobe analysis was carried out with a JEOL JXA-8900R at Okayama University of Science. Quantitative analyses were performed with 15 kV accelerating voltage, 12 nA beam current, and 3–5 μm beam size. Natural and synthetic silicates and oxides were used as standards for calibration. The CITZAF method (Armstrong, 1988) was employed for matrix corrections. Representative analyses are listed in Table 1. Fe was assumed to be Fe^{2+} unless otherwise noted.

Garnet

All of the garnet is zoned with spessartine-rich cores, except for garnet in the fine-grained jadeite eclogite (Fig. 7). X_{Mg} [= Mg/(Mg + Fe^{2+})] increases continuously from core to rim, but the nature of this trend varies with rock type. For example, the lowest X_{Mg} values are type I lawsonite eclogite (0.22), type II lawsonite eclogite/garnet-bearing lawsonite blueschist/garnet-bearing quartz–phengite schist (0.16–0.17), and jadeite eclogite (0.12–0.14). Reversely zoned rims, some with micron-scale oscillatory zoning, can be observed in some type I lawsonite eclogite, type II lawsonite eclogite, and garnet-bearing lawsonite blueschist (Fig. 7E). Garnet in coarse-grained jadeite eclogite has an almandine-rich composition: $alm_{55–76}grs_{17–28}prp_{0.8–10}sps_{0–22}$, with X_{Mg} = 0.02–0.12. Garnet in fine-grained jadeite eclogite has a spessartine-poor composition: $alm_{63–71}grs_{20–25}prp_{2–11}sps_{1–4}$, with X_{Mg} = 0.07–0.14; spessartine-rich cores were not observed. Garnet in the type I lawsonite eclogite is Ca and Mg rich relative to other rock types. It has a wider compositional range: $alm_{54–69}grs_{24–30}prp_{2–16}sps_{1–17}$, with X_{Mg} = 0.04–0.22; the highest X_{Mg} rim values are higher than in the other rock types. Garnet in type II lawsonite eclogite is $alm_{54–75}grs_{18–24}prp_{4–14}sps_{0.5–22}$, with X_{Mg} = 0.04–0.17; in some samples, the maximum X_{Mg} is similar to that in coarse-grained jadeite eclogite. Garnet in garnet-bearing lawsonite blueschist is $alm_{59–73}grs_{17–26}prp_{4–13}sps_{0.3–15}$, with X_{Mg} = 0.09–0.16. Poikiloblastic garnet in the garnet-bearing quartz–phengite schist is relatively poor in spessartine at the cores and has the composition: $alm_{63–72}grs_{18–24}prp_{4–13}sps_{0.3–7}$, with X_{Mg} = 0.05–0.16. In contrast, fine-grained garnet in garnet-bearing quartz–phengite schist is richer in spessartine: $alm_{49–68}grs_{16–22}prp_{3–12}sps_{4–31}$, with X_{Mg} = 0.05–0.15.

Clinopyroxene

Figure 8 shows clinopyroxene compositions from each rock type; the Fe^{2+}/Fe^{3+} ratio and end-member components were calculated following Harlow (1999). Jadeite eclogites contain a bimodal compositional distribution of omphacitic and jadeitic clinopyroxene. The coarse-grained jadeite eclogite contains two generations of sodic pyroxene (Tsujimori et al., 2005). The prograde jadeitic pyroxene (Jd-I) has a composition intermediate between jadeite and omphacite ($jd_{62–75}di+hd_{16–24}ae_{0–18}$; X_{Mg} = 0.09–0.93). Later-stage (blueschist-stage) jadeitic pyroxene (Jd-II) has a significantly higher jadeite component ($jd_{74–87}di + hd_{9–16}ae_{0–11}$; X_{Mg} = 0.30–0.90), and coexists with minor omphacite ($jd_{42–50}di + hd_{36–46}ae_{7–16}$; X_{Mg} = 0.70–0.88). Some Jd-I inclusions in garnet are also partly recrystallized into two pyroxenes. In contrast, the fine-grained jadeite eclogite contains two coexisting prograde pyroxenes: omphacite ($jd_{33–52}di + hd_{36–53}ae_{0.2–19}$; X_{Mg} = 0.58–0.97) and jadeite ($jd_{69–83}di + hd_{9–17}ae_{0–15}$; X_{Mg} = 0.47–1); the inclusion-rich green cores are slightly enriched in aegirine. Omphacite in type I lawsonite eclogite is $jd_{32–51}di + hd_{40–50}ae_{0–23}$; X_{Mg} ranges from 0.62 to 0.98. Omphacite inclusions within garnet are commonly enriched in aegirine, whereas recrystallized grains in the matrix are poor in aegirine. Omphacite in type II lawsonite eclogite is aegirine rich and jadeite poor relative to the other rock types ($jd_{25–44}di + hd_{37–52}ae_{5–30}$; X_{Mg} = 0.65–0.97). Some omphacite inclusions within garnet have a higher aegirine component than matrix omphacite. Omphacite in garnet-bearing lawsonite blueschist has similar compositions to that of type II lawsonite eclogite ($jd_{26–43}di + hd_{43–54}ae_{5–17}$; X_{Mg} = 0.69–0.94); the omphacite inclusions in garnet are rich in aegirine.

Amphiboles

Compositions of sodic amphibole are plotted in Figure 9; the structural formulae of amphiboles were calculated based on O = 23, and the Fe^{2+}/Fe^{3+} ratio was estimated with total cation = 13, excluding Ca, Na, and K. All sodic amphibole is low in Ca (0.02–0.25 p.f.u.) and ^{IV}Al (0–0.16 p.f.u.). The inferred $Fe^{3+}/(Fe^{3+} + Al)$ ratio is typically <0.2. Ferroglaucophane inclusions in garnet of coarse-grained lawsonite eclogite have a low X_{Mg} of 0.18–0.49. Prograde inclusions of ferroglaucophane and glaucophane with X_{Mg} = 0.46–0.52 were also found in garnet of garnet-bearing lawsonite blueschist. No compositional differences in glaucophane grown during the retrograde eclogite stage and blueschist stage were found; these amphiboles have high Al and X_{Mg} values. Glaucophane in the retrograde veins of type I lawsonite eclogite has X_{Mg} = 0.59–0.76, similar to matrix glaucophane in type II lawsonite eclogite (X_{Mg} = 0.62–0.70), garnet-bearing lawsonite blueschist (X_{Mg} = 0.63–0.72), and garnet-bearing quartz–phengite schist (X_{Mg} = 0.63–0.74). Retrograde actinolite replacing glaucophane in the garnet-bearing quartz–phengite schist has 0.21–0.41 ^{M4}Na, 0.15–0.20 ^{IV}Al (p.f.u.), and X_{Mg} = 0.81–0.86.

TABLE 1. REPRESENTATIVE MICROPROBE ANALYSES OF MINERALS FROM HIGH-PRESSURE ROCKS FROM THE CARRIZAL GRANDE AREA

Mineral		SiO_2	TiO_2	Al_2O_3	Cr_2O_3	FeO*	MnO	MgO	CaO	Na_2O	K_2O	Total	O=	Si	Ti	Al	Cr	Fe^{3+}	Fe^{2+}	Mn	Mg	Ca	Na	K	Total
JdEC (coarse-grained)																									
Grt	rim	37.8	0.1	21.1	0.0	31.6	0.1	2.1	8.1	0.1	0.0	100.9	*12*	3.00	0.00	1.97	0.00	0.00	2.09	0.01	0.24	0.69	0.01	0.00	8.01
Grt	rim	36.9	0.2	21.3	0.0	32.8	0.1	1.6	7.7	0.0	0.0	100.5	*12*	2.96	0.01	2.01	0.00	0.00	2.20	0.01	0.19	0.66	0.01	0.00	8.03
Grt	core	37.3	0.3	20.3	0.0	27.5	6.7	0.3	8.6	0.0	0.0	100.9	*12*	3.00	0.02	1.92	0.00	0.00	1.85	0.46	0.04	0.74	0.00	0.00	8.02
Jd	inc. G	57.2	0.0	16.8	0.0	6.0	0.1	2.8	5.9	11.7	0.0	100.5	*6*	1.99	0.00	0.69	0.00	0.13	0.04	0.00	0.14	0.22	0.79	0.00	4.00
Jd	Jd-I	57.6	0.1	17.4	0.0	5.6	0.1	2.3	5.1	12.0	0.0	100.2	*6*	2.00	0.00	0.71	0.00	0.09	0.07	0.00	0.12	0.19	0.81	0.00	4.00
Jd	Jd-I	57.4	0.1	17.0	0.0	5.4	0.0	2.8	5.6	11.7	0.0	99.9	*6*	2.00	0.00	0.70	0.00	0.09	0.07	0.00	0.14	0.21	0.79	0.00	4.00
Jd	Jd-II	58.2	0.1	20.3	0.0	3.7	0.1	1.5	2.9	13.1	0.0	99.7	*6*	2.01	0.00	0.82	0.00	0.03	0.08	0.00	0.08	0.11	0.87	0.00	4.00
Jd	Jd-II	57.8	0.1	19.9	0.0	4.2	0.0	1.5	3.1	13.1	0.0	99.6	*6*	2.00	0.00	0.81	0.00	0.07	0.05	0.00	0.08	0.11	0.88	0.00	4.00
Omp		56.0	0.0	10.7	0.0	6.5	0.0	6.8	11.7	8.0	0.0	99.9	*6*	1.99	0.00	0.45	0.00	0.12	0.08	0.00	0.36	0.45	0.55	0.00	4.00
Omp		55.8	0.1	10.9	0.0	7.6	0.0	6.1	11.3	8.2	0.0	100.0	*6*	1.99	0.00	0.46	0.00	0.12	0.10	0.00	0.32	0.43	0.56	0.00	4.00
Fgl	inc. G	56.2	0.0	11.5	0.0	17.1	0.1	5.3	0.3	7.4	0.0	97.9	*23*	7.94	0.00	1.91	0.00	0.07	1.95	0.01	1.12	0.05	2.03	0.00	15.08
Lws	inc. G	38.9	0.1	31.4	0.1	0.5	0.0	0.0	17.1	0.0	0.0	88.2	*8*	2.04	0.01	1.94	0.01	0.02	0.00	0.00	0.00	0.96	0.00	0.00	4.97
Lws		38.1	0.0	31.6	0.1	0.3	0.0	0.0	17.1	0.0	0.0	87.2	*8*	2.02	0.00	1.97	0.01	0.01	0.00	0.00	0.00	0.97	0.00	0.00	4.98
Phe	inc. G	53.3	0.2	24.1	0.0	3.1	0.0	4.5	0.0	0.2	8.9	94.4	*11*	3.56	0.01	1.90	0.00	0.00	0.17	0.00	0.45	0.00	0.02	0.76	6.87
Chl	inc. G	23.5	0.0	19.4	0.0	42.0	1.1	2.3	0.0	0.0	0.0	88.4	*28*	5.44	0.00	5.30	0.01	0.00	8.14	0.22	0.79	0.00	0.01	0.01	19.92
JdEC (fine-grained)																									
Grt	rim	37.7	0.0	21.5	0.1	28.6	1.3	2.6	8.2	0.0	0.0	100.1	*12*	2.99	0.00	2.01	0.00	0.00	1.89	0.09	0.31	0.70	0.01	0.00	8.01
Grt	rim	37.8	0.0	21.3	0.0	29.6	1.1	2.5	7.9	0.0	0.0	100.4	*12*	2.99	0.00	1.99	0.00	0.00	1.96	0.08	0.30	0.67	0.00	0.00	8.01
Grt	core	37.8	0.1	21.3	0.0	30.6	1.6	1.3	8.4	0.0	0.0	101.1	*12*	3.00	0.01	1.99	0.00	0.00	2.03	0.11	0.15	0.71	0.00	0.00	8.00
Jd		57.2	0.2	17.8	0.0	5.4	0.2	2.5	4.1	12.0	0.0	99.4	*6*	2.00	0.00	0.73	0.00	0.07	0.09	0.01	0.13	0.15	0.81	0.00	4.00
Omp	rim	56.2	0.0	11.5	0.0	5.3	0.0	6.8	12.2	7.8	0.0	99.9	*6*	2.00	0.00	0.48	0.00	0.05	0.10	0.00	0.36	0.47	0.53	0.00	4.00
Omp	core	55.4	0.1	9.1	0.0	8.5	0.0	7.1	13.3	7.0	0.0	100.4	*6*	1.98	0.00	0.38	0.00	0.13	0.12	0.00	0.38	0.51	0.49	0.00	4.00
Lws		38.6	0.1	32.1	0.0	0.3	0.1	0.0	17.1	0.0	0.0	88.2	*8*	2.02	0.00	1.98	0.00	0.01	0.00	0.00	0.00	0.96	0.00	0.00	4.98
Phe		54.4	0.2	23.0	0.0	2.3	0.0	5.2	0.0	0.2	9.1	94.5	*11*	3.62	0.01	1.80	0.00	0.00	0.13	0.00	0.51	0.00	0.02	0.77	6.87
Type I LwEC																									
Grt	rim	38.5	0.0	21.7	0.1	25.6	0.2	4.0	9.5	0.0	0.0	99.5	*12*	3.02	0.00	2.01	0.01	0.00	1.67	0.01	0.47	0.79	0.00	0.00	7.98
Grt	rim	38.3	0.0	21.6	0.1	26.6	0.2	4.2	9.1	0.0	0.0	100.0	*12*	3.00	0.00	1.99	0.01	0.00	1.74	0.01	0.49	0.76	0.00	0.00	8.01
Grt	core	37.3	0.1	20.7	0.0	32.0	1.7	1.1	7.2	0.0	0.0	100.0	*12*	3.01	0.01	1.97	0.00	0.00	2.16	0.11	0.13	0.62	0.00	0.00	8.00
Grt	outer r.	38.3	0.1	21.4	0.0	28.7	0.1	3.4	8.6	0.0	0.0	100.6	*12*	3.01	0.00	1.98	0.00	0.00	1.88	0.01	0.39	0.72	0.00	0.00	8.00
Omp	inc. G	55.6	0.2	8.7	0.1	10.2	0.2	6.0	11.2	8.2	0.0	100.4	*6*	1.99	0.01	0.37	0.00	0.20	0.10	0.01	0.32	0.43	0.57	0.00	4.00
Omp		55.9	0.0	10.7	0.1	6.5	0.1	6.7	11.3	8.3	0.0	99.6	*6*	1.99	0.00	0.45	0.00	0.14	0.06	0.00	0.35	0.43	0.57	0.00	4.00
Omp		56.0	0.1	10.5	0.0	6.3	0.0	7.1	12.0	7.8	0.0	99.9	*6*	1.99	0.00	0.44	0.00	0.11	0.08	0.00	0.37	0.46	0.54	0.00	4.00
Lws	inc. G	38.4	0.1	31.3	0.1	1.3	0.0	0.0	17.4	0.0	0.0	88.6	*8*	2.02	0.00	1.93	0.00	0.05	0.00	0.00	0.00	0.98	0.00	0.00	4.99
Lws		38.1	0.0	31.2	0.1	0.5	0.0	0.0	17.3	0.0	0.0	87.3	*8*	2.02	0.00	1.95	0.00	0.02	0.00	0.00	0.00	0.98	0.00	0.00	4.99
Pmp	inc. L	36.2	0.6	23.1	0.1	8.3	0.2	0.9	22.3	0.2	0.0	91.7	*24.5*	6.05	0.07	4.54	0.01	0.00	1.16	0.02	0.21	4.00	0.07	0.00	16.14
Chl	inc. G	28.2	0.1	19.1	0.0	20.8	0.3	18.2	0.1	0.0	0.0	86.8	*28*	5.83	0.01	4.66	0.00	0.00	3.61	0.06	5.62	0.03	0.00	0.00	19.82
Phe		50.7	0.1	25.5	0.0	3.4	0.0	3.7	0.0	0.1	10.0	93.6	*11*	3.45	0.01	2.05	0.00	0.00	0.20	0.00	0.37	0.00	0.02	0.87	6.96

(continued)

TABLE 1. REPRESENTATIVE MICROPROBE ANALYSES OF MINERALS FROM HIGH-PRESSURE ROCKS FROM THE CARRIZAL GRANDE AREA *(continued)*

Mineral		SiO_2	TiO_2	Al_2O_3	Cr_2O_3	FeO*	MnO	MgO	CaO	Na_2O	K_2O	Total	O=	Si	Ti	Al	Cr	Fe^{3+}	Fe^{2+}	Mn	Mg	Ca	Na	K	Total
Type II LwEC																									
Grt	rim	38.2	0.0	21.3	0.0	28.8	0.7	3.2	7.9	0.0	0.0	100.2	*12*	3.02	0.00	1.98	0.00	1.90	0.05	0.37	0.67	0.00	0.00	8.00	15.99
Grt	core	37.3	0.2	20.7	0.0	26.0	7.2	0.8	8.1	0.0	0.0	100.3	*12*	3.00	0.01	1.96	0.00	0.00	1.75	0.49	0.10	0.70	0.00	0.00	8.01
Grt	outer r.	37.9	0.1	21.5	0.0	30.7	1.7	2.6	6.4	0.0	0.0	101.0	*12*	3.00	0.00	2.00	0.00	0.00	2.03	0.12	0.30	0.54	0.01	0.00	8.00
Omp	inc. G	55.0	0.0	7.8	0.1	9.8	0.0	6.9	11.9	7.8	0.0	99.3	*6*	1.99	0.00	0.33	0.00	0.23	0.06	0.00	0.37	0.46	0.55	0.00	4.00
Omp		55.5	0.0	8.0	0.0	9.8	0.0	6.6	11.0	8.4	0.0	99.3	*6*	2.00	0.00	0.34	0.00	0.24	0.05	0.00	0.36	0.42	0.58	0.00	4.00
Omp		56.0	0.0	10.1	0.0	7.2	0.0	6.6	11.5	8.0	0.0	99.4	*6*	2.01	0.00	0.43	0.00	0.11	0.10	0.00	0.35	0.44	0.56	0.00	4.00
Gln		58.2	0.0	11.2	0.0	10.5	0.0	9.8	0.4	7.4	0.0	97.4	*23*	7.99	0.00	1.81	0.00	0.14	1.07	0.00	2.00	0.05	1.97	0.00	15.03
Lws	inc. G	38.1	0.1	30.5	0.0	1.4	0.0	0.0	17.4	0.0	0.0	87.5	*8*	2.03	0.00	1.91	0.00	0.00	0.06	0.00	0.00	0.99	0.00	0.00	4.99
Lws		37.7	0.1	30.7	0.0	1.3	0.0	0.0	16.9	0.0	0.0	86.8	*8*	2.02	0.00	1.93	0.00	0.00	0.05	0.00	0.00	0.97	0.00	0.00	4.98
Chl	inc. G	25.7	0.0	18.2	0.0	32.8	0.5	10.4	0.0	0.0	0.0	87.7	*28*	5.65	0.00	4.73	0.00	0.00	6.05	0.10	3.43	0.00	0.02	0.01	19.99
Phe		52.5	0.2	23.9	0.0	3.6	0.0	4.3	0.0	0.3	10.1	94.8	*11*	3.53	0.01	1.89	0.00	0.00	0.20	0.00	0.43	0.00	0.04	0.86	6.96
Grt-LwBS																									
Grt	rim	37.7	0.1	21.3	0.0	30.5	0.3	3.3	6.8	0.0	0.0	99.9	*12*	2.99	0.00	2.00	0.00	0.00	2.03	0.02	0.39	0.58	0.00	0.00	8.01
Grt	core	37.7	0.1	20.8	0.0	28.3	4.5	1.0	8.4	0.0	0.0	100.9	*12*	3.01	0.01	1.96	0.00	0.00	1.89	0.30	0.12	0.72	0.00	0.00	8.01
Omp	inc. G	54.8	0.0	7.9	0.0	8.3	0.0	7.8	13.5	6.7	0.0	99.0	*6*	1.99	0.00	0.34	0.00	0.15	0.11	0.00	0.42	0.52	0.47	0.00	4.00
Omp		56.0	0.0	10.2	0.0	6.3	0.1	7.2	12.0	7.7	0.0	99.6	*6*	2.00	0.00	0.43	0.00	0.10	0.09	0.00	0.38	0.46	0.54	0.00	4.00
Omp		55.2	0.0	7.5	0.0	8.5	0.0	7.9	14.2	6.5	0.0	99.8	*6*	2.00	0.00	0.32	0.00	0.14	0.11	0.00	0.42	0.55	0.45	0.00	4.00
Gln		58.4	0.0	10.5	0.0	9.6	0.0	10.7	0.4	7.4	0.0	97.1	*23*	8.00	0.00	1.70	0.00	0.21	0.89	0.00	2.18	0.06	1.95	0.00	15.01
Lws	inc. G	38.5	0.0	31.4	0.0	0.6	0.0	0.0	17.5	0.0	0.0	88.2	*8*	2.02	0.00	1.95	0.00	0.03	0.00	0.00	0.00	0.99	0.00	0.00	4.99
Lws		38.2	0.0	31.4	0.1	0.5	0.0	0.0	17.5	0.0	0.0	87.8	*8*	2.02	0.00	1.96	0.00	0.02	0.00	0.00	0.00	0.99	0.00	0.00	4.99
Chl	inc. G	26.1	0.0	18.6	0.0	31.5	0.4	10.5	0.2	0.0	0.0	87.3	*28*	5.73	0.00	4.80	0.00	0.00	5.79	0.08	3.43	0.04	0.00	0.00	19.87
Phe	inc. G	54.0	0.1	22.8	0.0	2.7	0.0	4.3	0.1	0.1	9.9	94.0	*11*	3.63	0.01	1.81	0.00	0.00	0.15	0.00	0.43	0.00	0.02	0.85	6.89
Phe		52.5	0.1	23.2	0.1	3.4	0.1	4.1	0.1	0.2	10.2	93.8	*11*	3.56	0.01	1.86	0.00	0.00	0.19	0.00	0.41	0.01	0.02	0.88	6.95
Grt-Qtz-Phe schist																									
Grt-L	rim	37.6	0.0	21.2	0.0	30.8	0.5	2.5	7.2	0.0	0.0	99.9	*12*	3.00	0.00	1.99	0.00	2.06	0.00	0.04	0.30	0.61	0.00	0.00	8.00
Grt-L	core	37.3	0.1	21.2	0.0	31.2	1.6	1.1	7.6	0.1	0.0	100.1	*12*	2.99	0.01	2.01	0.00	2.09	0.00	0.11	0.13	0.65	0.01	0.00	8.00
Grt-S		37.5	0.1	21.0	0.0	25.3	9.0	1.2	6.4	0.0	0.0	100.5	*12*	3.01	0.00	1.98	0.00	1.70	0.00	0.61	0.14	0.55	0.01	0.00	8.00
Gln		58.1	0.1	11.4	0.0	10.5	0.0	9.3	0.1	7.5	0.0	97.0	*23*	8.01	0.01	1.85	0.00	0.10	1.12	0.00	1.92	0.02	1.99	0.00	15.01
Lws	inc. G	37.8	0.2	31.5	0.0	0.5	0.0	0.0	17.5	0.0	0.0	87.5	*8*	2.00	0.01	1.97	0.00	0.02	0.00	0.00	0.00	0.99	0.00	0.00	4.99
Lws		38.6	0.1	32.1	0.0	0.2	0.0	0.0	17.4	0.0	0.0	88.4	*8*	2.02	0.00	1.98	0.00	0.01	0.00	0.00	0.00	0.97	0.00	0.00	4.99
Pmp	inc. L	36.6	0.1	24.5	0.0	3.8	0.8	2.2	22.3	0.1	0.0	90.4	*24.5*	6.07	0.01	4.78	0.00	0.00	0.53	0.11	0.55	3.96	0.04	0.01	16.06
Phe		53.5	0.2	24.0	0.1	2.3	0.0	4.3	0.0	0.2	9.2	93.8	*11*	3.58	0.01	1.90	0.00	0.00	0.13	0.00	0.43	0.00	0.02	0.78	6.86

FeO* = total Fe as Fe^{2+}. See text for calculation of Fe^{3+}/Fe^{2+} ratio of clinopyroxene.
inc. G = inclusion in garnet; inc. L = inclusion in lawsonite; outer r. = outermost rim
Grt-L = porphyroblastic garnet in Grt-Qtz-Phe schist; Grt-S = small garnet in Grt-Qtz-Phe schist.

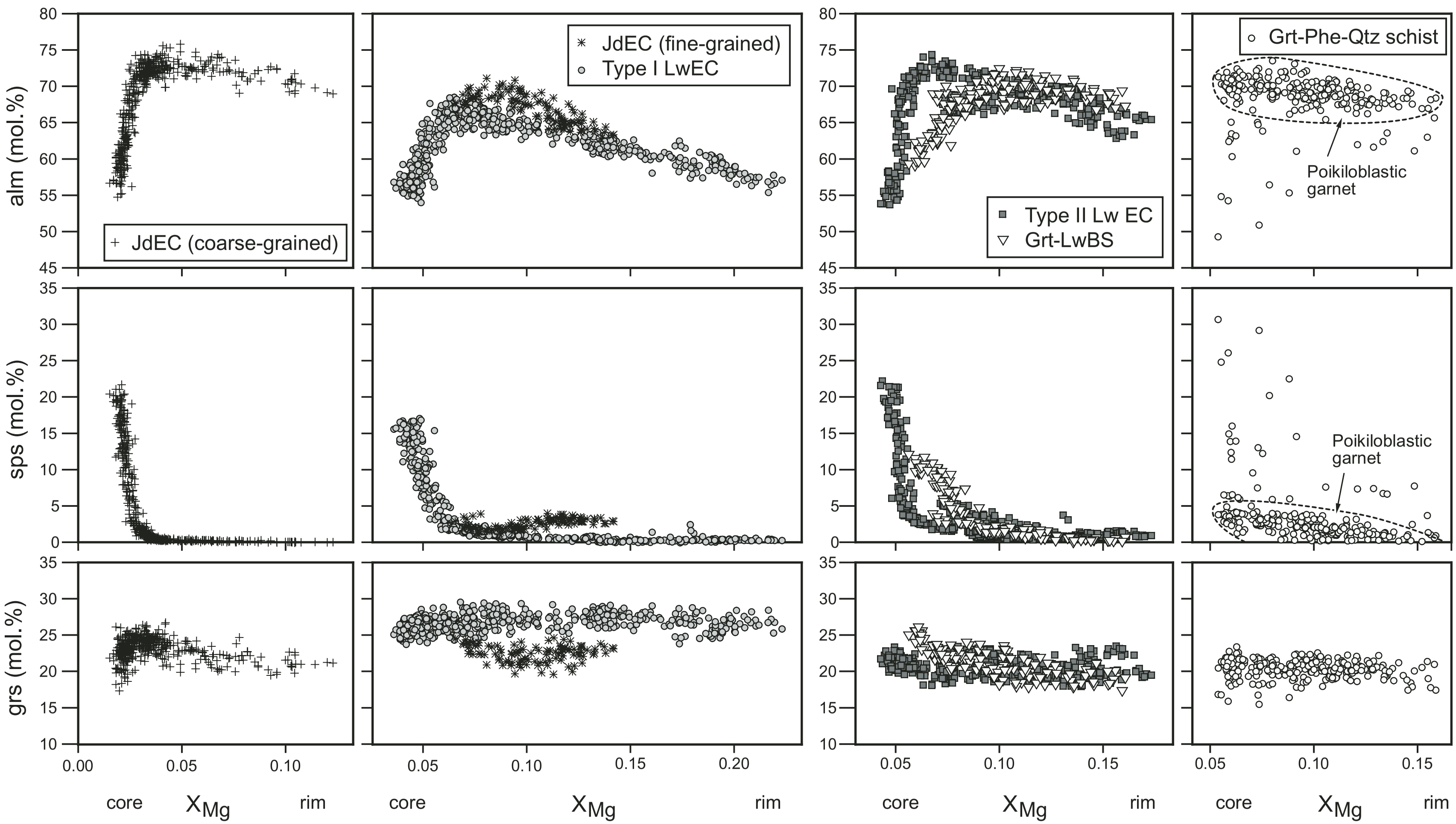

Figure 7. Compositional trends of garnet in high-pressure rocks from Carrizal Grande. Grt-Qtz-Phe schist—garnet-bearing quartz–phengite schist; LwEC—lawsonite eclogite; Grt-LwBS—garnet-bearing lawsonite blueschist; JdEC—jadeite eclogite; grs—grossular, sps—spessartine; alm—almandine.

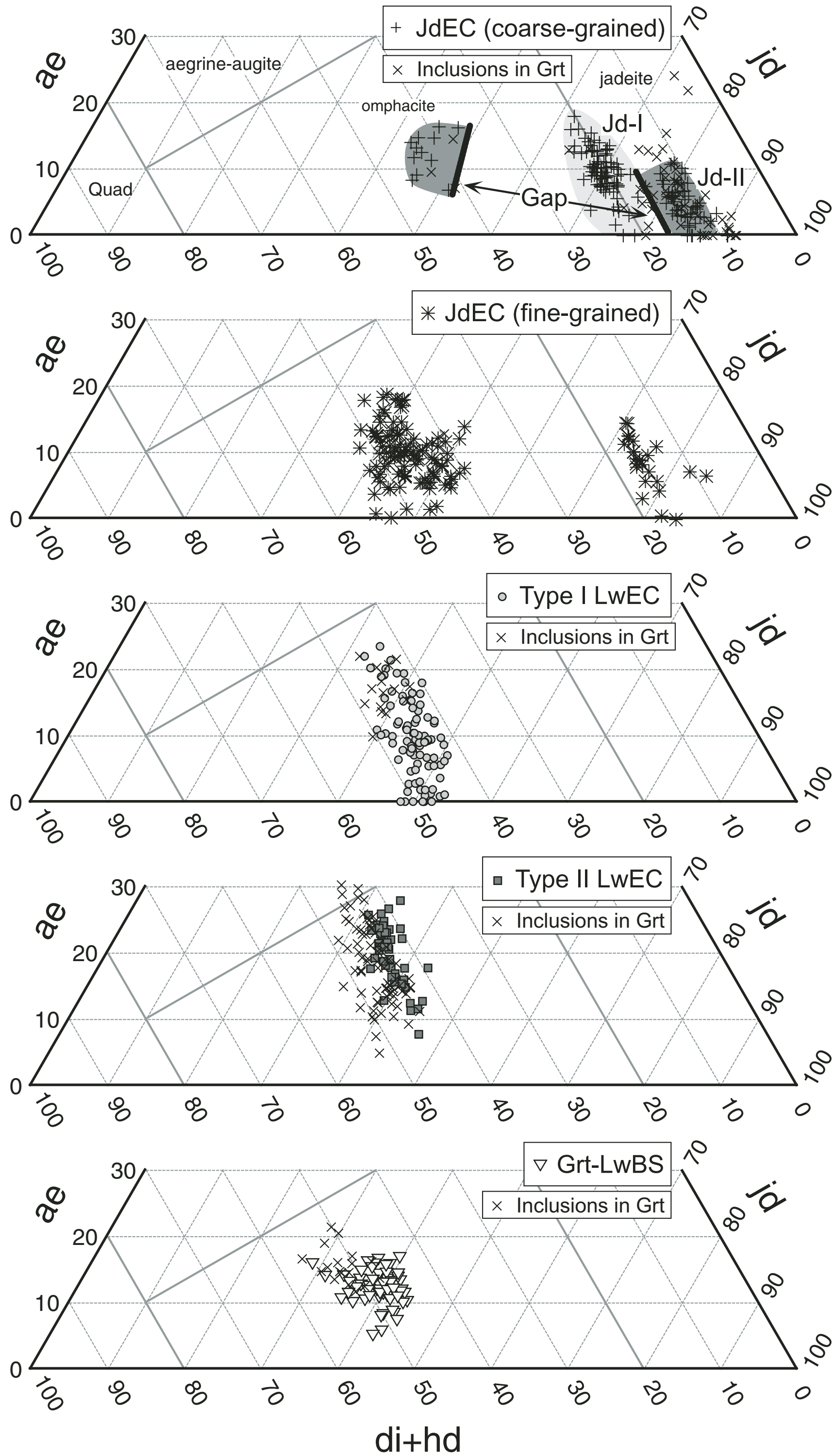

Figure 8. Compositional trends of clinopyroxene in high-pressure rocks from Carrizal Grande. LwEC—lawsonite eclogite; Grt-LwBS—garnet-bearing lawsonite blueschist; JdEC—jadeite eclogite; jd—jadeite; ae—aegirine; di + hd—diopside plus hedenbergite.

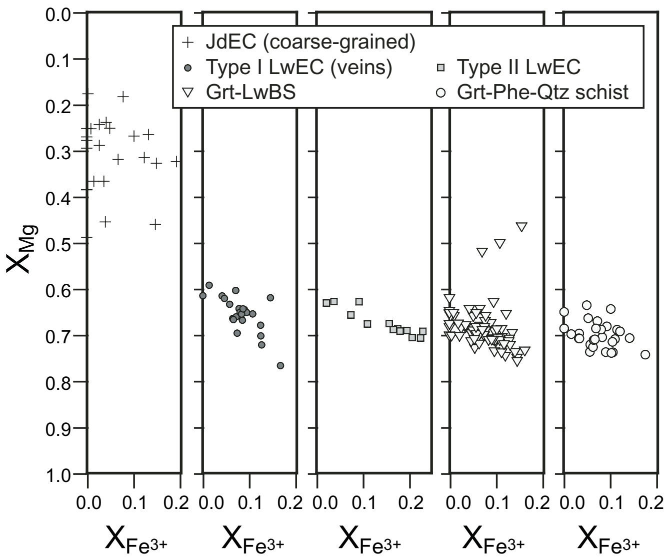

Figure 9. Compositional variations of sodic amphibole in high-pressure rocks from Carrizal Grande. Grt-Qtz-Phe schist—garnet-bearing quartz–phengite schist; LwEC—lawsonite eclogite; Grt-LwBS—garnet-bearing lawsonite blueschist; JdEC—jadeite eclogite.

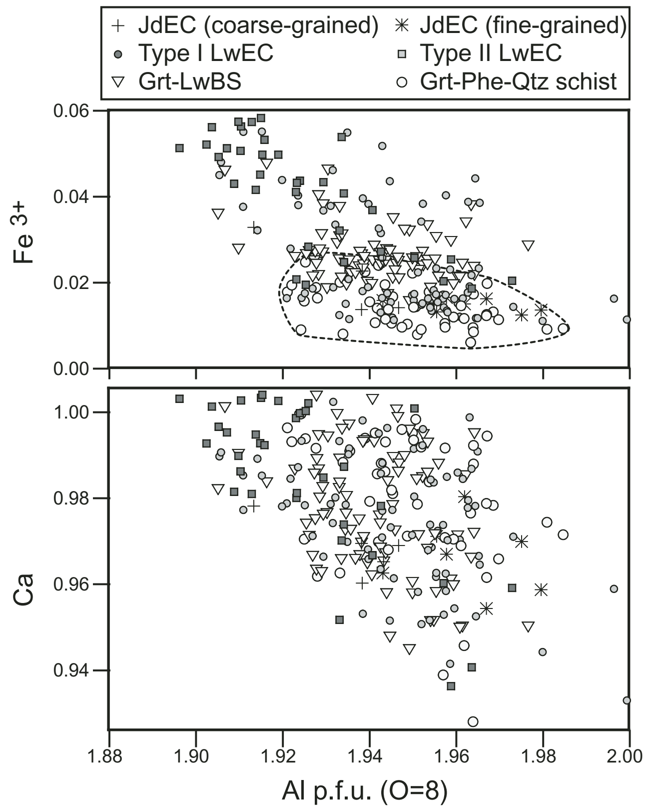

Figure 10. Compositional variation of lawsonite in high-pressure rocks from Carrizal Grande. Grt-Qtz-Phe schist—garnet-bearing quartz–phengite schist; LwEC—lawsonite eclogite; Grt-LwBS—garnet-bearing lawsonite blueschist; JdEC—jadeite eclogite.

Lawsonite

The compositions of lawsonite are plotted in Figure 10; all Fe is assumed to be Fe^{3+}. The lawsonite has 0.01–0.06 Fe^{3+}, 1.90–2.00 Al, and 0.93–1.00 Ca p.f.u. of 8 oxygen. The $Fe^{3+}/(Fe^{3+} + Al)$ ratio ranges from 0.003 to 0.03. There is no systematic chemical zoning, however, a negative correlation between Al and Fe^{3+} suggests substitution of Fe^{3+} for Al in the octahedral site. There are no compositional differences between different textural types of lawsonite within the same sample. Lawsonite in garnet-bearing quartz–phengite schist contains a significantly lower Fe^{3+} concentration, consistent with the occurrence of graphite.

Chlorite

Chlorite shows a wide compositional variation that varies with rock type (Fig. 11). Mn content has a good negative correlation with X_{Mg}. Chlorite inclusions in garnet in coarse-grained jadeite eclogite are low in X_{Mg} (0.09–0.10) and Si (5.4–5.5), and high in Al (5.2–5.3 p.f.u.), in contrast to other rock types (X_{Mg} = 0.30–0.70 and 4.4–5.1 Al p.f.u.). The X_{Mg} values increase from type I lawsonite eclogite (0.48–0.70) to type II lawsonite eclogite/garnet-bearing lawsonite blueschist/garnet-bearing quartz–phengite schist (0.30–0.52) to jadeite eclogite (0.12–0.14).

Phengite

Phengite in the investigated rocks has a wide compositional range with high Si (3.45–3.65 p.f.u.) and low $Na/(Na^{+}K)$ (0.01–0.06); X_{Mg} varies from 0.63 to 0.82 (Fig. 12). There are no apparent differences in composition among different textural types of phengite in individual samples. However, late-stage phengite in the type I lawsonite eclogite is relatively low in Si.

Pumpellyite

Pumpellyite inclusions within lawsonite of type I lawsonite eclogite and garnet-bearing quartz–phengite schist are Al rich, with Al/(Al + Fe + Mg) = 0.78–0.88, and contain 0.09–0.21 wt% Na_2O (Fig. 13). Pumpellyite in type I lawsonite eclogite is less magnesian (X_{Mg} = 0.15–0.16) than in the garnet-bearing quartz–phengite schists (X_{Mg} = 0.51–0.55).

Other Minerals

Ilmenite inclusions in the cores of garnet in coarse-grained jadeite eclogite and type II lawsonite eclogite contain 2.8–7 wt% MnO. Titanite in the mafic rock types contains 0.6–1.2 wt% Al_2O_3, whereas rare titanite in garnet-bearing quartz–phengite schist contains <2.5 wt% Al_2O_3. Stilpnomelane in type II lawsonite eclogite and garnet-bearing lawsonite blueschist has X_{Mg} = 0.36–0.40.

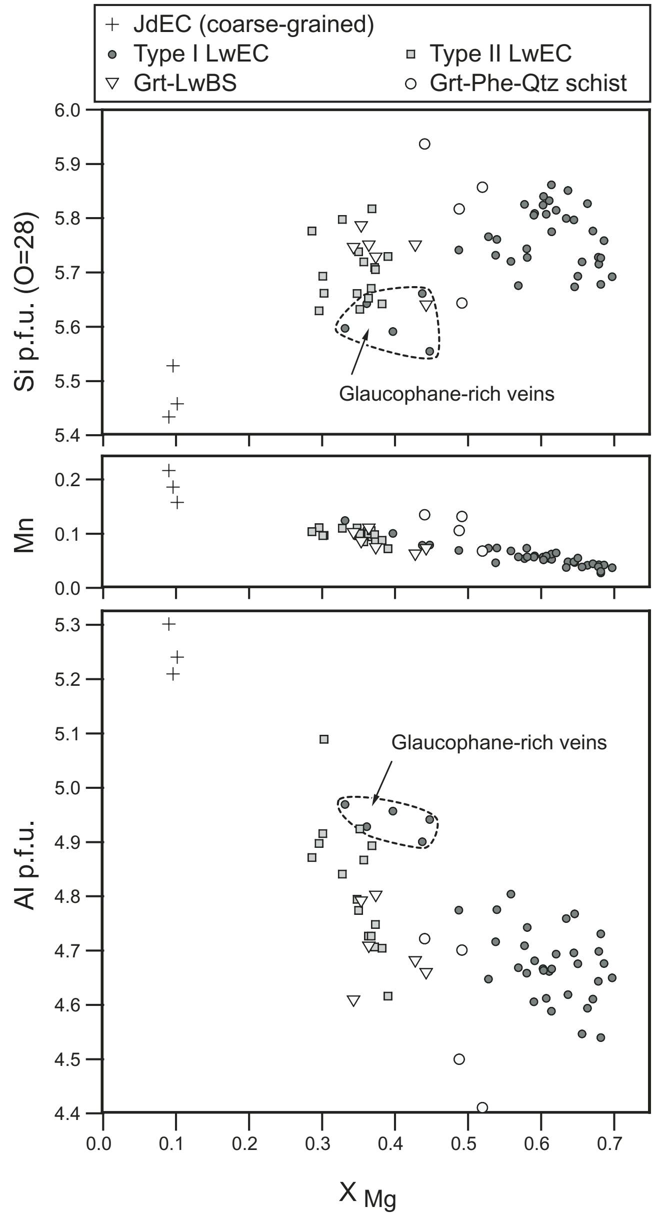

Figure 11. Compositional variations of chlorite in high-pressure rocks from Carrizal Grande. Grt-Qtz-Phe schist—garnet-bearing quartz–phengite schist; LwEC—lawsonite eclogite; Grt-LwBS—garnet-bearing lawsonite blueschist; JdEC—jadeite eclogite.

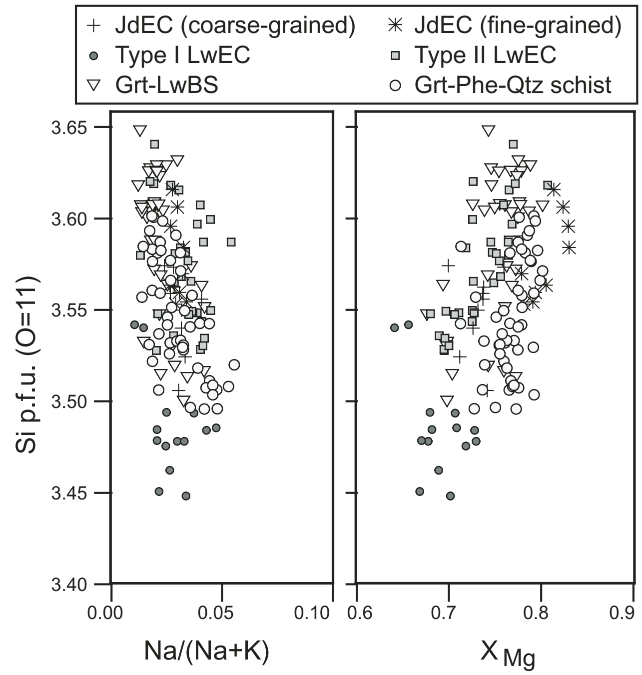

Figure 12. Compositional variations of phengite in high-pressure rocks from Carrizal Grande. Grt-Qtz-Phe schist—garnet-bearing quartz–phengite schist; LwEC—lawsonite eclogite; Grt-LwBS—garnet-bearing lawsonite blueschist; JdEC—jadeite eclogite.

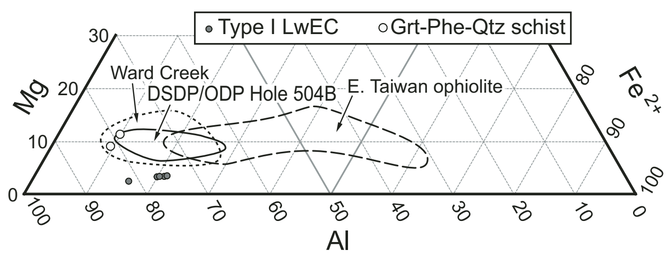

Figure 13. Compositional variations of pumpellyite in high-pressure rocks from Carrizal Grande. Compositional fields of pumpellyite from the Ward Creek blueschist (Maruyama and Liou, 1987), ocean-floor basalt of Deep Sea Drilling Project (DSDP)/Ocean Drilling Program (ODP) Hole 504B (Ishizuka, 1999), and East Taiwan ophiolite (Liou, 1979) are also shown. Grt-Qtz-Phe schist—garnet-bearing quartz–phengite schist; LwEC—lawsonite eclogite.

P-T CONDITIONS OF METAMORPHISM

The *P-T* conditions for each metamorphic stage can be constrained through the use of phase equilibria, thermobarometry, and petrogenetic grids. In this study, calculations to obtain phase equilibria were carried out using version 3.25 of THERMOCALC (Powell et al., 1998); the activities of mineral end members for calculations were obtained using the AX program of T.J.B. Holland (http://www.earthsci.unimelb.edu.au/tpg/thermocalc/). Characteristic features for each stage are described below.

Prograde Eclogite Stage

The prograde eclogite-facies assemblage is Grt + Omp (or Jd) + Lws + Chl + Rt + Qtz ± Ilm ± Fgl ± Phe in mafic rock types. As described in the preceding section, the X_{Mg} of garnet increases continuously from spessartine-rich cores to almandine-rich rims. This implies a progressive increase in temperature during the growth of garnet by consumption of chlorite (e.g., Enami, 1998; Inui and Toriumi, 2004). Rutile and lawsonite are ubiquitous garnet inclusions in all rock types, and ilmenite occurs in the cores of some garnets in type I lawsonite eclogite. The lower temperature for garnet with lawsonite inclusions is limited by the equilibrium:

$$3\ \text{Lws}\ [CaAl_2Si_2O_7(OH)_2{\cdot}H_2O] + 2\ \text{Fe-Tlc} = 2\ \text{Alm}\ [Fe_3Al_2Si_3O_{12}] + \text{Grs}\ [Ca_3Al_2Si_3O_{12}] + 5\ \text{Qtz}\ [SiO_2] + 8\ H_2O\ \text{(Okay, 2002).} \quad (1)$$

The absence of talc suggests a minimum temperature around 290–300 °C for the core compositions of eclogitic garnets with S_1 or S_2 for this reaction (Fig. 14A). The presence of Lws + Rt + Ilm in the garnet core suggests that the metamorphic temperature is limited by the equilibria:

$$\text{Lws}\ [CaAl_2Si_2O_7(OH)_2{\cdot}H_2O] + 2\ \text{Ttn}\ [CaTiSiO_5] = \text{Grs}\ [Ca_3Al_2Si_3O_{12}] + 2\ \text{Rt}\ [TiO_2] + \text{Qtz}\ [SiO_2] + 2\ H_2O \quad (2)$$

and

$$3\ \text{Lws}\ [CaAl_2Si_2O_7(OH)_2{\cdot}H_2O] + 6\ \text{Ilm}\ [FeTiO_3] + 3\ \text{Qtz}\ [SiO_2] = 6\ \text{Rt}\ [TiO_2] + 2\ \text{Alm}\ [Fe_3Al_2Si_3O_{12}] + \text{Grs}\ [Ca_3Al_2Si_3O_{12}] + 6\ H_2O. \quad (3)$$

This constraint indicates a metamorphic temperature of ~380–390 °C for the garnet core in coarse-grained jadeite eclogite (Fig. 14A). Moreover, the presence of Jd + Lws + Rt and the absence of paragonite in the jadeite eclogite constrain the pressure ($P > 1.4$ GPa at $T = {\sim}400$ °C) with the reactions (Fig. 14A):

$$\text{Jd} + 4\ \text{Lws}\ [CaAl_2Si_2O_7(OH)_2{\cdot}H_2O] = 2\ \text{Czo}\ [Ca_2Al_3Si_3O_{12}(OH)] + \text{Pg}\ [Na_2Al_4(Si_6Al_2)O_{20}(OH)_4] + \text{Qtz}\ [SiO_2] + 6\ H_2O \quad (4)$$

(Ghent et al., 1993), and

$$\text{Jd} + \text{Lws}\ [CaAl_2Si_2O_7(OH)_2{\cdot}H_2O] + \text{Rt}\ [TiO_2] = \text{Pg}\ [Na_2Al_4(Si_6Al_2)O_{20}(OH)_4] + \text{Ttn}\ [CaAl_2Si_2O_7(OH)_2{\cdot}H_2O] + 2\ H_2O\ \text{(Okay, 2002).} \quad (5)$$

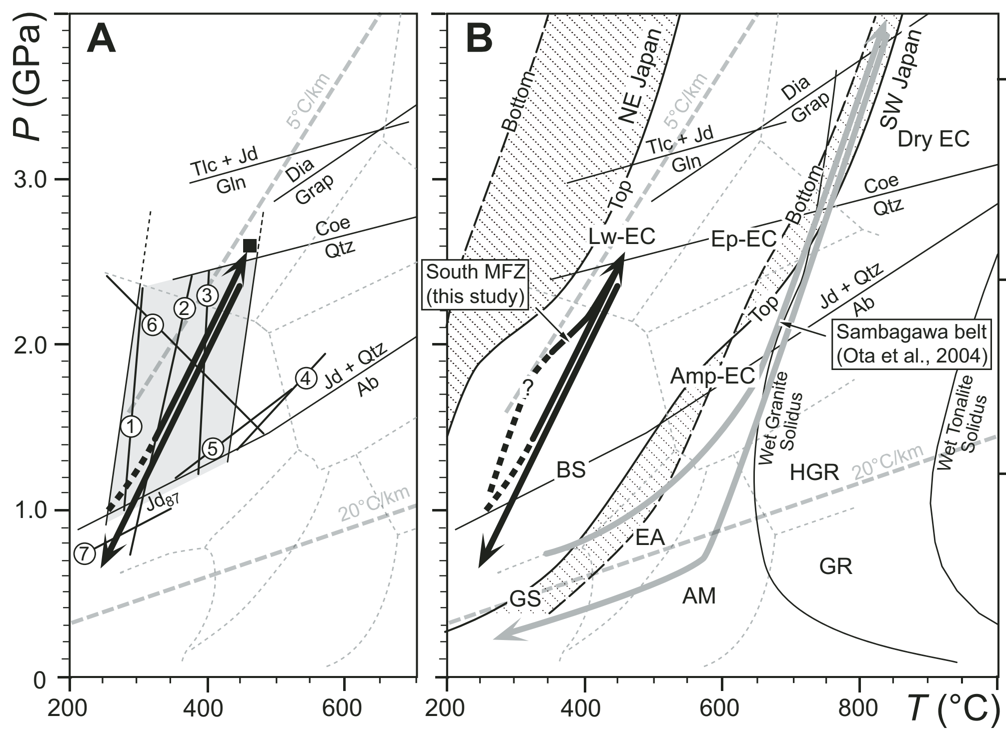

Figure 14. Qualitative pressure-temperature (*P-T*) path of lawsonite eclogite from Carrizal Grande. (A) Selected reaction curves to constrain metamorphic conditions. Numbered reactions are discussed in the text. Gray area represents the *P-T* field of the prograde eclogite stage constrained by the Jd + Qtz = Ab equilibria (Holland, 1983), and garnet-clinopyroxene thermometry (Krogh Ravna, 2000). (B) Comparisons of *P-T* path for Guatemalan lawsonite eclogite (this study) with the inferred *P-T* path of the highest-grade rocks of the Sanbagawa metamorphic belt (gray arrows: Ota et al., 2004) and *P-T* conditions for oceanic crust beneath present-day NE Japan (cold) and SW Japan (warm) subduction zones (hachured areas: Peacock and Wang, 1999). The metamorphic facies and their abbreviations are after Liou et al. (2004). MFZ—Motagua fault zone, EC—eclogite.

In coarse-grained lawsonite eclogite, the equilibrium

$$\text{Pg } [Na_2Al_4(Si_6Al_2)O_{20}(OH)_4] + 2\text{ Fgl } [Na_2Fe_3Al_2Si_8O_{22}(OH)_2] = 6\text{ Jd } [NaAlSi_2O_6] + 2\text{ Alm } [Fe_3Al_2Si_3O_{12}] + 4\text{ Qtz } [SiO_2] + 4\ H_2O \text{ (Miyazaki et al., 1998)} \quad (6)$$

further limits the minimum pressure to >1.6–2.0 GPa at temperature to ~350–450 °C for the Grt + Jd + Fgl assemblage (Tsujimori et al., 2005) (Fig. 14A). The Fe^{2+}-Mg distribution between omphacite and garnet also provides geothermobarometric information. The change in the Fe^{2+}-Mg distribution coefficient (K_D) between omphacite inclusions and adjacent garnet basically decreases from core to rim, suggesting heating during growth. The peak thermal condition was achieved at the highest X_{Mg} portion of the garnet rims within the lawsonite stability field (Figs. 5E and 7). A summary of the garnet-clinopyroxene thermometry at 2 GPa, applying the calibration of Krogh Ravna (2000), is shown in Figure 15: at P = 2.0 GPa, T = 290–490 °C (Fig. 14A). A relatively wide range of variations might be caused from the Fe^{2+}/Fe^{3+} estimation of omphacite and incomplete equilibrium between omphacite inclusions with adjacent garnet. Although the omphacite and garnet may not have achieved equilibrium at these low temperatures, the preservation of pumpellyite in lawsonite supports this low-T interpretation (e.g., Schiffman and Liou, 1980, 1983). Garnet-clinopyroxene-phengite thermobarometry (Krogh Ravna and Terry, 2004) of composite mineral inclusions in garnet rims near the highest X_{Mg} portion in the coarse-grained jadeite eclogite, and of matrix pairs in fine-grained jadeite eclogite, yields a maximum P = ~2.4–2.6 at T = ~480 °C (Fig. 14A). Therefore, it is likely that eclogitization initiated at T = ~300 °C and P > 1.1 GPa, and continued to T = ~480 °C and P = ~2.6 GPa.

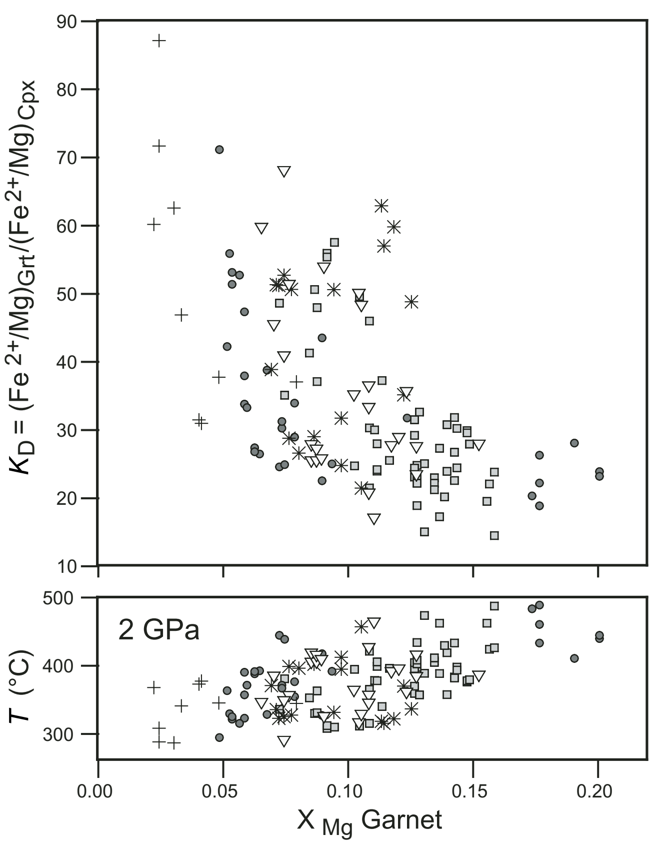

Figure 15. Relationships between X_{Mg} of garnet and K_D of garnet (Grt) + coexisting clinopyroxene (Cpx) inclusions and temperature at P = 2 GPa. Temperature was calculated using the garnet-clinopyroxene thermobarometer of Krogh Ravna (2000).

Retrograde Eclogite Stage

Folding of the pre-existing S_2 foliation and formation of the S_3 foliation accompanied the retrograde eclogite stage. The mineral assemblage is best preserved in type II lawsonite eclogite and garnet-bearing lawsonite blueschist, and has reversely zoned garnet rims and Omp ± Gln + Lws + Rt + Qtz ± Phe within S_3; these glaucophanes and lawsonites contain rutile inclusions. Garnet-clinopyroxene-phengite thermobarometry (Krogh Ravna and Terry, 2004) yields P = ~1.8 GPa and T = ~400 °C (Fig. 14A). It may be improbable that garnet grew during retrogression at such low T, however, retrograde garnet growth with a distinct X_{Mg} drop at the outermost rims has been described from eastern Alpine (Hoschek, 2001) and Sanbagawa eclogites (Ota et al., 2004). In a simplified Al_2O_3-CaO-MgO system with five phases (Lws, Chl, Prp, Grs, and Di) and excess Qtz and H_2O, the phase rule specifies a single invariant point and five univariant curves. Among these curves, a garnet-forming reaction within the stability field of Di + Grt (Prp +Grs):

$$3\text{ Lws } [CaAl_2Si_2O_7(OH)_2{\cdot}H_2O] + 3\text{ Di } [CaMgSi_2O_6] = 2\text{ Grs } [Ca_3Al_2Si_3O_{12}] + \text{Prp } [Fe_3Al_2Si_3O_{12}] + 3\text{ Qtz } [SiO_2] + 6\ H_2O \quad (7)$$

has a positive dP/dT slope of ~0.2 GPa/100 °C for garnet ($prp_{10}grs_{25}$) and omphacite (di_{35}). Therefore minor retrograde garnet overgrowth may be explained by this reaction.

Blueschist Stage

The late blueschist-facies assemblage is Gln + Lws + Chl + Phe + Ttn + Qtz ± Ab. No Fe-Mg exchange geothermobarometer is applicable to the observed mineral assemblage, however, this paragenesis suggests T < 300 °C (e.g., Maruyama and Liou, 1988; Evans, 1990. In coarse-grained jadeite eclogite, the retrograde assemblage Jd-II ± Omp + Ttn + Chl + Qtz ± Ab may represent this same stage. The simultaneous growth of two clinopyroxenes with a wide compositional gap and the Jd + Qtz = Ab sliding equilibrium (equation 7) (Holland, 1983) suggest approximate P-T conditions of P = ~0.7 GPa and T <~300 °C (Tsujimori et al., 2005) (Fig. 14A).

DISCUSSION

P-T-D Paths of Subduction and Exhumation

Detailed petrologic and microstructural examination of various high-pressure rock types in the Carrizal Grande area constrains the *P-T*-deformation (D) history during the subduction and exhumation of the eclogitized oceanic crust. As described herein, there are four deformational stages: D_1, D_2, D_3, and D_4; D_3 was the dominant stage.

The D_1–D_2 stages correspond to prograde eclogite stages, and D_3 represents a retrograde eclogite stage. The *P-T* constraints suggest that eclogitization during the D_1–D_2 stage initiated at T = ~300 °C and P > 1.1 GPa and continued to T = ~480 °C and P = ~2.6 GPa (Fig. 14). This prograde eclogitization was accompanied by ductile to partly brittle deformation.

In contrast, the D_3 stage, with P = ~1.8 GPa and T = ~400 °C, postdates the thermal maximum, because S_3 minerals are texturally in equilibrium with reversely zoned garnet rims that lack the S_2 fabric.

Furthermore, hydration and blueschist-facies recrystallization at shallower levels occurred in the high-pressure rocks of the Carrizal Grande area; the breakdown of rutile is critical to defining this later stage. The development of the blueschist-facies hydration was heterogeneous, limited by fluid introduction, seen as irregular-shaped glaucophane-rich hydrous veins. However, it appears to have been coeval with the minor but ubiquitous D_4 deformation defined by open folds, crenulations, and shear. The D_4 deformation may have affected the serpentinite associated with the high-pressure rocks. Metasomatic rocks, such as jadeitite, omphacitite, lawsonite-jadeite rock, and omphacite-glaucophane rock, are closely associated with the serpentinite and high-pressure rocks (e.g., Harlow, 1994; Harlow et al., 2003; Harlow and Sorensen, 2005). The available petrologic information for these metasomatic rocks suggests that they were synchronous with the blueschist-facies stage and accompanying D_4 deformation. Formation of the serpentinite mélange then postdated D_4.

As shown in Figure 14B, the inferred *P-T* trajectory lies near a geotherm of ~5 °C km^{-1}, i.e., near the "forbidden zone" of Liou et al. (2000), and shows a characteristic hairpin-like path. Such a *P-T* path suggests that the rocks were refrigerated during exhumation such that no greenschist- or amphibolite-facies recrystallization took place. The eclogitized oceanic crust was thus most likely exhumed up a subduction channel, and then trapped in serpentinite at shallow levels (<40 km), where the lawsonite blueschist developed.

Eclogitization in a Cold Subduction Zone

According to the calculated steady-state thermal structure of subduction zones (e.g., Peacock and Wang, 1999; Peacock, 2001), phase relationships in the MORB + H_2O system (e.g., Kerrick and Connolly, 2001; Hacker et al., 2003a, 2003b), and high-pressure experiments of the MORB + H_2O system (e.g., Schmidt and Poli, 1998; Okamoto and Maruyama, 1999; Spandler et al., 2003), the eclogitization of oceanic crust within Pacific-type subduction zones is likely to take place in the lawsonite stability field. Although the occurrence of lawsonite eclogite in orogenic belts is extremely rare (Tsujimori et al., 2006), the discovery of coesite-bearing lawsonite eclogite xenoliths on the Colorado Plateau (Usui et al., 2003) supports the hypothesis of lawsonite eclogite formation in Pacific-type subduction zones.

What are the implications of lawsonite eclogitization in cold subduction zones? Lawsonite can accommodate up to 11.5 wt% H_2O plus Sr, rare earth elements (REEs), and Pb, and is stable in cold subduction zones to at least 300 km depth (e.g., Schmidt, 1995; Pawley, 1994; Okamoto and Maruyama, 1999). Consequently, the dehydration of lawsonite likely plays an important role in the generation of arc magmatism, slab seismicity, and the recycling of volatiles and high field strength elements into mantle (Schmidt and Poli, 1998; Kerrick and Connolly, 2001; Connolly and Kerrick, 2002; Hacker et al., 2003a, 2003b; Spandler et al., 2003; Rüpke et al., 2004). Intermediate-depth earthquakes (50–300 km in depth) may be triggered by dehydration of the descending oceanic plate (Kirby et al., 1996; Helffrich, 1996; Peacock and Wang, 1999; Peacock and Hyndman, 1999; Peacock, 2001; Dobson et al., 2002; Omori et al., 2002; Hacker et al., 2003a, 2003b; Yamasaki and Seno, 2003).

How do the petrologic observations of this study fit with the calculated thermal and petrologic structure of cold subduction zones? For example, the thermal structure of the NE Japan subduction zone (Peacock and Wang, 1999; Hacker et al., 2003b) is shown in Figure 16. Present-day NE Japan is a cold subduction zone where the 130 Ma Pacific plate is subducting beneath the Eurasian plate at 91 mm/yr (Peacock and Wang, 1999). Figure 16 shows that the inferred prograde *P-T* trajectory of the Guatemalan lawsonite eclogite is slightly hotter than the calculated *P-T* conditions of the oceanic crust beneath NE Japan (Peacock and Wang, 1999). However, our *P-T* estimates for the initiation of eclogitization (T = ~300 °C and P > 1.1 GPa) and metamorphic peak (T = ~480 °C and P = ~2.6 GPa) are nearly consistent with the thermal structure of Peacock and Wang (1999) (Fig. 16). Our inferred prograde *P-T* path lies within the jadeite–lawsonite blueschist and lawsonite–amphibole eclogite fields of Hacker et al. (2003b) (Fig. 16). Zhang et al. (2004) reported high Vp/Vs ratios (~1.79–1.81) within the oceanic crust at 60–100 km depth beneath NE Japan, and interpreted this as a mixture of blueschist and eclogite.

What are the realistic dehydration reactions producing earthquakes within the slab crust? The experimental study by Okamoto and Maruyama (1999) showed a continuous lawsonite-consuming dehydration reaction within the lawsonite eclogite field. If lawsonite breakdown occurs, the grossular component in the crystallizing garnet should increase; in fact lawsonite

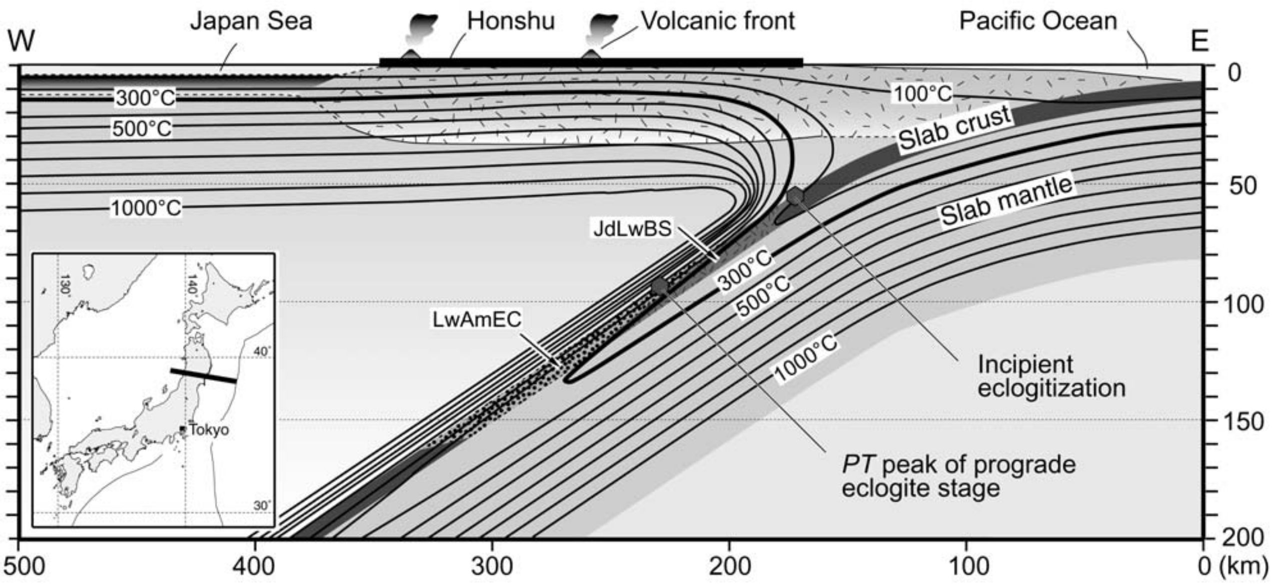

Figure 16. Thermal structure of the NE Japan subduction zone (Peacock and Wang, 1999; Hacker et al., 2003b) is similar to the prograde pressure-temperature (*P-T*) trajectory for Guatemalan lawsonite eclogite. The areas marked JdLwBS and LwAmEC represent jadeite lawsonite blueschist and lawsonite amphibole eclogite fields of Hacker et al. (2003a, 2003b). Isotherm contour interval is 100 °C.

eclogite xenoliths from the Colorado Plateau show this change (Helmstaedt and Schulze, 1988; Usui et al., 2003). In the Guatemalan lawsonite eclogites, the grossular component is essentially constant or decreases slightly from core to rim (Fig. 7). This indicates that the chlorite-consuming reactions to form almandine-pyrope-spessartine garnet were more effective than the lawsonite-consuming reaction to form the grossular component. At ~100 km depth in cold subduction zones, dehydration-induced seismicity may be caused by these chlorite-consuming reactions.

ACKNOWLEDGMENTS

This research was supported by the Japanese Society for the Promotion of Science through Research Fellowship for Research Abroad of the first author (Tsujimori). The authors acknowledge support by the National Science Foundation through grants EAR-0003355 and EAR-0510325 (Liou), EAR-0309320 (Harlow and Sorensen), and EAR-0309321 (Sisson). Tsujimori thanks Robert Coleman, William Rohtert, John Cleary, and Pieter Lee for their guidance during a field trip to Guatemala. We also thank Dick Mandell for alerting us to the presence of abundant eclogite uncovered by Hurricane Mitch. Thomas Zack, John Goodge, Roberto Compagnoni, and Bradley Hacker critically reviewed this manuscript.

REFERENCES CITED

Abbott, R.N., Draper, G., and Keshav, S., 2005, UHP magma paragenesis, garnet peridotite, and garnet clinopyroxenite: An example from the Dominican Republic: International Geology Review, v. 47, p. 233–247.

Altherr, R., Topuz, G., Marschall, H., Zack, T., and Ludwig, T., 2004, Evolution of a tourmaline-bearing lawsonite-eclogite from the Elekdag area (central Pontides, N Turkey): Evidence for infiltration of slab-derived B-rich fluids during exhumation: Contributions to Mineralogy and Petrology, v. 148, p. 409–425.

Armstrong, J.T., 1988, Quantitative analysis of silicate and oxide minerals: Comparison of Monte Carlo, ZAF and Phi-Rho-Z procedures, *in* Newbury, D.E., ed., Analysis microbeam: San Francisco, California, San Francisco Press, p. 239–246.

Beccaluva, L., Bellia, S., Coltorti, M., Dengo, G., Giunta, G., Mendez, J., Romero, J., Rotolo, S., and Siena, F., 1995, The northwestern border of the Caribbean plate in Guatemala: New geological and petrological data on the Motagua ophiolitic belt: Ofioliti, v. 20, p. 1–15.

Caron, J.-M., and Péquignot, G., 1986, The transition between blueschists and lawsonite-bearing eclogites based on observations from Corsican metabasites: Lithos, v. 19, p. 205–218, doi: 10.1016/0024-4937(86)90023-X.

Caron, J.-M., Kiénast, J.-R., and Triboulet, C., 1981, High-pressure/low-temperature metamorphism and polyphase Alpine deformation at Sant'Andrea di Cotone (eastern Corsica, France): Tectonophysics, v. 78, p. 419–451, doi: 10.1016/0040-1951(81)90023-8.

Clarke, G.L., Atchison, J.C., and Cluzel, D., 1997, Eclogites and blueschists of the Pam Peninsula, NE New Caledonia: A reappraisal: Journal of Petrology, p. 38, p. 843–876.

Connolly, J.A.D., and Kerrick, D.M., 2002, Metamorphic controls on seismic velocity of subducted oceanic crust at 100–250 km depth: Earth and Planetary Science Letters, v. 204, p. 61–74, doi: 10.1016/S0012-821X(02)00957-3.

Dobson, D.P., Meredith, P.G., and Boon, S.A., 2002, Simulation of subduction zone seismicity by dehydration of serpentinite: Science, v. 298, p. 1407–1410, doi: 10.1126/science.1075390.

Draper, G., 1986, Blueschists and associated rocks in eastern Jamaica and their significance for Cretaceous plate-margin development in the northern Caribbean: Geological Society of America Bulletin, v. 97, p. 48–60, doi: 10.1130/0016-7606(1986)97<48:BAARIE>2.0.CO;2.

Enami, M., 1998, Pressure-temperature path of Sanbagawa prograde metamorphism deduced from grossular zoning of garnet: Journal of Metamorphic Geology, v. 16, p. 97–106, doi: 10.1111/j.1525-1314.1998.00058.x.

Evans, B.W., 1990, Phase relations of epidote-blueschists: Lithos, v. 25, p. 3–23, doi: 10.1016/0024-4937(90)90003-J.

Francis, A.H., 2005, Deformation history of the Maya and Chortís blocks: Insight to the evolution of the Motagua fault zone, Guatemala [M.S. thesis]: Houston, Rice University, 149 p.

Francis, A.H., Avé Lallemant, H.G., and Sisson, V.B., 2005, Tectonic history of two disparate high-pressure, low-temperature metamorphic belts along the Motagua fault zone, Guatemala: Geological Society of America Abstracts with Programs, v. 37, no. 3, p. 5.

Ghent, E.D., Stout, M.Z., and Erdmer, P., 1993, Pressure-temperature evolution of lawsonite-bearing eclogites, Pinchi Lake, British Columbia: Journal of Metamorphic Geology, v. 11, p. 279–290.

Giaramita, M.J., and Sorensen, S.S., 1994, Primary fluids in low-temperature eclogites: Evidence from two subduction complexes (Dominican Republic, and California, USA): Contributions to Mineralogy and Petrology, v. 117, p. 279–292, doi: 10.1007/BF00310869.

Gonçalves, P., Guillot, S., Lardeaux, J.M., Nicollet, C., and Mercier de Lepinay, B., 2000, Thrusting and sinistral wrenching in a pre-Eocene HP-LT Caribbean accretionary wedge (Samana Peninsula, Dominican Republic): Geodinamica Acta, v. 13, p. 119–132, doi: 10.1016/S0985-3111(00)00116-9.

Green, D.H., Lockwood, J.P., and Kiss, E., 1968, Eclogite and almandine-jadeite-quartz rock from the Guajira Peninsula, Colombia, South America: The American Mineralogist, v. 53, p. 1320–1335.

Hacker, B.R., Abers, G.A., and Peacock, S.M., 2003a, Subduction factory 1. Theoretical mineralogy, densities, seismic wave speeds, and H_2O contents: Journal of Geophysical Research, v. 108, no. 2029, doi: 10.1029/2001JB001127.

Hacker, B.R., Peacock, S.M., Abers, G.A., and Holloway, S., 2003b, Subduction factory 2. Intermediate-depth earthquakes in subducting slabs are linked to metamorphic dehydration reactions: Journal of Geophysical Research, v. 108, 2030, doi: 10.1029/2001JB001129.

Harlow, G.E., 1994, Jadeitites, albitites and related rocks from the Motagua fault zone, Guatemala: Journal of Metamorphic Geology, v. 12, p. 49–68.

Harlow, G.E., 1999, Interpretation of Kcpx and CaEs components in clinopyroxene from diamond inclusions and mantle samples, *in* Gurney, J.J., Gurney, J.L., Pascoe, M.D., and Richardson, S.H., eds., Proceedings of Seventh International Kimberlite Convention: Cape Town, Redroof Design Company, vol. I, p. 321–331.

Harlow, G.E., and Sorensen, S.S., 2005, Jade (nephrite and jadeitite) and serpentinite: Metasomatic connections: International Geology Review, v. 47, p. 113–146.

Harlow, G.E., Sisson, V.B., Avé Lallemant, H.G., Sorensen, S.S., and Seitz, R., 2003, High-pressure, metasomatic rocks along the Motagua fault zone, Guatemala: Ofioliti, v. 28, p. 115–120.

Harlow, G.E., Hemming, S.R., Avé Lallemant, H.G., Sisson, V.B., and Sorensen, S.S., 2004, Two high-pressure–low-temperature serpentinite-matrix mélange belts, Motagua fault zone, Guatemala: A record of Aptian and Maastrichtian collisions: Geology, v. 32, p. 17–20, doi: 10.1130/G19990.1.

Helffrich, G., 1996, Subducted lithospheric slab velocity structure: Observations and mineralogical inferences, *in* Bebout, G.E., Scholl, D., Kirby, S., and Platt, J.P., eds., Subduction: Top to bottom: American Geophysical Union Geophysical Monograph 96, p. 215–222.

Helmstaedt, H., and Schulze, D.J., 1988, Eclogite-facies ultramafic xenoliths from Colorado Plateau diatreme breccias: Comparison with eclogites in crystal environments, evaluation of the subduction hypothesis, and implications for eclogite xenoliths from diamondiferous kimberlites, *in* Smith, D.C., ed., Eclogite and eclogite facies rocks: New York, Elsevier Science, p. 387–450.

Hirajima, T., Banno, S., Hiroi, Y., and Ohta, Y., 1988, Phase petrology of eclogites and related rocks from the Motalafjella high-pressure metamorphic complex in Spitsbergen and its significance: Lithos, v. 22, p. 75–97, doi: 10.1016/0024-4937(88)90018-7.

Holland, T.J.B., 1983, The experimental determination of activities in disordered and short-range ordered jadeitic pyroxenes: Contributions to Mineralogy and Petrology, v. 82, p. 214–220, doi: 10.1007/BF01166616.

Hoschek, G., 2001, Thermobarometry of metasediments and metabasites from the eclogite zone of the Hohe Tauern, eastern Alps, Austria: Lithos, v. 59, p. 127–150, doi: 10.1016/S0024-4937(01)00063-9.

Inui, M., and Toriumi, M., 2004, A theoretical study on the formation of growth zoning in garnet consuming chlorite: Journal of Petrology, v. 45, p. 1369–1392, doi: 10.1093/petrology/egh016.

Ishizuka, H., 1999, Pumpellyite from the oceanic crust, DSDP/ODP Hole 504B: Mineralogical Magazine, v. 63, p. 891–900, doi: 10.1180/002646199548998.

Kerrick, D.M., and Connolly, J.A.D., 2001, Metamorphic devolatilization of subducted oceanic metabasites: Implications for seismicity, arc magmatism and volatile recycling: Earth and Planetary Science Letters, v. 189, p. 19–29, doi: 10.1016/S0012-821X(01)00347-8.

Kirby, S.H., Stein, S., Okal, E.O., and Rubie, D.C., 1996, Metastable mantle phase transformations and deep earthquakes in subducting oceanic lithosphere: Reviews of Geophysics, v. 34, p. 261–306, doi: 10.1029/96RG01050.

Kretz, R., 1983, Symbols for rock-forming minerals: The American Mineralogist, v. 68, p. 277–279.

Krogh Ravna, E., 2000, The garnet-clinopyroxene Fe^{2+}-Mg geothermometer: An updated calibration: Journal of Metamorphic Geology, v. 18, p. 211–219, doi: 10.1046/j.1525-1314.2000.00247.x.

Krogh Ravna, E., and Terry, M.P., 2004, Geothermobarometry of UHP and HP eclogites and schists—An evaluation of equilibria among garnet-clinopyroxene-kyanite-phengite-coesite/quartz: Journal of Metamorphic Geology, v. 22, p. 579–592.

Liou, J.G., 1979, Zeolite facies metamorphism of basaltic rocks from the East Taiwan ophiolite: The American Mineralogist, v. 64, p. 1–14.

Liou, J.G., Hacker, B.R., and Zhang, R.Y., 2000, Into the forbidden zone: Science, v. 287, p. 1215–1216, doi: 10.1126/science.287.5456.1215.

Liou, J.G., Tsujimori, T., Zhang, R.Y., Katayama, I., and Maruyama, S., 2004, Global UHP metamorphism and continental subduction/collision: The Himalayan model: International Geology Review, v. 46, p. 1–27.

Maruyama, S., and Liou, J.G., 1988, Petrology of Franciscan metabasites along the jadeite-glaucophane type facies series, Cazadero, California: Journal of Petrology, v. 29, p. 1–37.

Maruyama, S., and Liou, J.G., 2005, From snowball to Phanerozoic Earth: International Geology Review, v. 47, p. 775–791.

McBirney, A., Aoki, K., and Bass, M.N., 1967, Eclogites and jadeite from the Motagua fault zone, Guatemala: The American Mineralogist, v. 52, p. 908–918.

Miyazaki, K., Sopaheluwakan, J., Zulkarnain, I., and Wakita, K., 1998, A jadeite-quartz-glaucophane rock from Karangsambung, central Java, Indonesia: The Island Arc, v. 7, p. 223–230, doi: 10.1046/j.1440-1738.1998.00164.x.

Och, D.J., Leitch, E.C., Caprarelli, G., and Watanabe, T., 2003, Blueschist and eclogite in tectonic mélange, Port Macquarie, New South Wales, Australia: Mineralogical Magazine, v. 67, p. 609–624, doi: 10.1180/0026461036740121.

Oh, C.W., Liou, J.G., and Maruyama, S., 1991, Low-temperature eclogites and eclogitic schists in Mn-rich metabasites in Ward Creek, California; Mn and Fe effects on the transition between blueschist and eclogite: Journal of Petrology, v. 32, p. 275–301.

Okamoto, K., and Maruyama, S., 1999, The high-pressure synthesis of lawsonite in the MORB + H_2O system: The American Mineralogist, v. 84, p. 362–373.

Okay, A.I., 2002, Jadeite-chloritoid-glaucophane-lawsonite blueschists in northwest Turkey: Unusually high P/T ratios in continental crust: Journal of Metamorphic Geology, v. 20, p. 757–768, doi: 10.1046/j.1525-1314.2002.00402.x.

Omori, S., Kamiya, S., Maruyama, S., and Zhao, D., 2002, Morphology of the intraslab seismic zone and devolatilization phase equilibria of the subducting slab peridotite: Earthquake Research Institute Bulletin, v. 76, p. 455–478.

Ortega-Gutiérrez, F., Solari, L.A., Solé, J., Martens, U., Gómez-Tuena, A., Morán-Ical, S., Reyes-Salas, M., and Ortega-Obregón, C., 2004, Polyphase, high-temperature eclogite-facies metamorphism in the

Chuacús Complex, central Guatemala: Petrology, geochronology, and tectonic implications: International Geology Review, v. 46, p. 445–470.

Ota, T., Terabayashi, M., and Katayama, I., 2004, Thermobaric structure and metamorphic evolution of the Iratsu eclogite body in the Sanbagawa belt, central Shikoku, Japan: Lithos, v. 73, p. 95–126, doi: 10.1016/j.lithos.2004.01.001.

Parkinson, C.D., Miyazaki, K., Wakita, K., Barber, A.J., and Carswell, D.A., 1998, An overview and tectonic synthesis of the pre-Tertiary very-high-pressure metamorphic and associated rocks of Java, Sulawesi, and Kalimantan, Indonesia: The Island Arc, v. 7, p. 184–200, doi: 10.1046/j.1440-1738.1998.00184.x.

Pawley, A.R., 1994, The pressure and temperature stability limits of lawsonite: Implications for H_2O recycling in subduction zones: Contributions to Mineralogy and Petrology, v. 118, p. 99–108, doi: 10.1007/BF00310614.

Pawley, A.R., Redfern, S.A.T., and Holland, T.J.B., 1996, Volume behavior of hydrous minerals at high pressure and temperature: I. Thermal expansion of lawsonite, zoisite, clinozoisite, and diaspore: The American Mineralogist, v. 81, p. 335–340.

Peacock, S.M., 2001, Are the lower planes of double seismic zones caused by serpentine dehydration in subducting oceanic mantle?: Geology, v. 29, p. 299–302, doi: 10.1130/0091-7613(2001)029<0299:ATLPOD>2.0.CO;2.

Peacock, S.M., and Hyndman, R.D., 1999, Hydrous minerals in the mantle wedge and the maximum depth of subduction thrust earthquakes: Geophysical Research Letters, v. 26, p. 2517–2520.

Peacock, S.M., and Wang, K., 1999, Seismic consequences of warm versus cool subduction metamorphism: Examples from southwest and northeast Japan: Nature, v. 286, p. 937–939.

Poli, S., and Schmidt, M.W., 1995, Water transport and release in subduction zones: Experimental constraints on basaltic and andesitic systems: Journal of Geophysical Research, v. 100, p. 22,299–22,314, doi: 10.1029/95JB01570.

Powell, R., Holland, T.J.B., and Worley, B., 1998, Calculating phase diagrams involving solid solutions via non-linear equations, with examples using THERMOCALC: Journal of Metamorphic Geology, v. 16, p. 577–588.

Rumble, D., Liou, J.G., and Jahn, B.M., 2003, Continental crust subduction and ultrahigh-pressure metamorphism, *in* Rudnick R.L., ed., The crust, Volume 3, Treatise on geochemistry (Holland, H.D., and Turekian, K.K., eds.): Oxford, Elsevier, p. 293–319.

Rüpke, L.H., Morgan, J.P., Hort, M., and Connolly, J.A.D., 2004, Serpentine and the subduction zone water cycle: Earth and Planetary Science Letters, v. 223, p. 17–34, doi: 10.1016/j.epsl.2004.04.018.

Schiffman, P., and Liou, J.G., 1980, Synthesis and stability relations of Mg-Al pumpellyite, $Ca_4Al_5MgSi_6O_{21}(OH)_7$: Journal of Petrology, v. 21, p. 441–474.

Schiffman, P., and Liou, J.G., 1983, Synthesis of Fe-pumpellyite and its stability relations with epidote: Journal of Metamorphic Geology, v. 1, p. 91–101.

Schmidt, M.W., 1995, Lawsonite: Upper pressure stability and formation of higher density hydrous phases: The American Mineralogist, v. 80, p. 1286–1292.

Schmidt, M.W., and Poli, S., 1998, Experimentally based water budgets for dehydrating slabs and consequences for arc magma generation: Earth and Planetary Science Letters, v. 163, p. 361–379, doi: 10.1016/S0012-821X(98)00142-3.

Schneider, J., Bosch, D., Monie, P., Guillot, S., Carcía-Casco, A., Lardeaux, J.M., Torres-Roldán, L., and Trujillo, G.M., 2004, Origin and evolution of the Escambray Massif (central Cuba): An example of HP/LT rocks exhumed during intraoceanic subduction: Journal of Metamorphic Geology, v. 22, p. 227–247, doi: 10.1111/j.1525-1314.2004.00510.x.

Shibakusa, H., and Maekawa, H., 1997, Lawsonite-bearing eclogitic metabasites in the Cazadero area, northern California: Mineralogy and Petrology, v. 61, p. 163–180, doi: 10.1007/BF01172482.

Sisson, V.B., Ertan, I.E., and Avé Lallemant, H.G., 1997, High pressure (~200 MPa) kyanite- and glaucophane-bearing schist and eclogite from the Cordillera de la Cost belt, Venezuela: Journal of Petrology, v. 38, p. 65–83, doi: 10.1093/petrology/38.1.65.

Sisson, V.B., Harlow, G.E., Sorensen, S.S., Brueckner, H.K., Sahm, E., Hemming, S., and Avé Lallemant, H.G., 2003, Lawsonite eclogite and other high-pressure assemblages in the southern Motagua fault zone, Guatemala: Implications for Chortís collision and subduction zones: Geological Society of America Abstracts with Programs, v. 35, no. 6, p. 639.

Sisson, V.B., Avé Lallemant, H.G., Ostos, M., Blythe, A.E., Snee, L.W., Copeland, P., Wright, J.E., Donelick, R.A., and Guth, L.R., 2005, Overview of radiometric ages in three allochthonous belts of northern Venezuela: Old ones, new ones, and their impact on regional geology, *in* Avé Lallemant, H.G., and Sisson, V.B., eds., Caribbean/South American plate interactions: Geological Society of America Special Paper 394, p. 91–117.

Smith, C.A., Sisson, V.B., Avé Lallemant, H.G., and Copeland, P., 1999, Two contrasting pressure-temperature-time paths in the Villa de Cura blueschist belt, Venezuela: Possible evidence for Late Cretaceous initiation of subduction in the Caribbean: Geological Society of America Bulletin, v. 111, p. 831–848, doi: 10.1130/0016-7606(1999)111<0831:TCPTTP>2.3.CO;2.

Smith, D.C., and Gendron, F., 1997, New locality and a new kind of jadeite jade from Guatemala; rutile-quartz-jadeitite: Fifth International Eclogite Conference: Terra Nova, Abstract supplement, no. 1, v. 9, p. 35.

Somin, M.L., Arakelyants, M.M., and Kolesnikov, E.M., 1992, Age and tectonic significance of high-pressure metamorphic rocks of Cuba: International Geology Review, v. 34, p. 105–118.

Sorensen, S.S., Grossman, J.N., and Perfit, M.R., 1997, Phengite-hosted LILE enrichment in eclogite and related rocks: Implications for fluid mediated mass transfer in subduction zones and arc magma genesis: Journal of Petrology, v. 38, p. 3–34.

Sorensen, S.S., Sisson, V.B., and Avé Lallemant, H.G., 2005, Geochemical evidence for possible trench provenance and fluid-rock histories, Cordillera de la Costa eclogite belt, Venezuela, *in* Avé Lallemant, H.G., and Sisson, V.B., eds., Caribbean/South American plate interactions: Geological Society of America Special Paper 394. p. 173–192.

Spandler, C., Hermann, J., Arculus, R., and Mavrogenes, J.A., 2003, Redistribution of trace elements during prograde metamorphism from lawsonite blueschist to eclogite facies; implications for deep subduction-zone processes: Contributions to Mineralogy and Petrology, v. 146, p. 205–222, doi: 10.1007/s00410-003-0495-5.

Stöckhert, B., Maresch, W.V., Brix, M., Kaiser, C., Toetz, A., Kluge, R., and Krückhans-Lueder, G., 1995, Crustal history of Margarita Island (Venezuela) in detail: Constraint on the Caribbean plate-tectonic scenario: Geology, v. 23, p. 787–790.

Tsujimori, T., Liou, J.G., and Coleman, R.G., 2005, Coexisting retrograde jadeite and omphacite in a jadeite-bearing lawsonite eclogite from the Motagua fault zone, Guatemala: The American Mineralogist, v. 90, p. 836–842, doi: 10.2138/am.2005.1699.

Tsujimori, T., Sisson, V.B., Liou, J.G., Harlow, G.E., and Sorensen, S.S., 2006, Very low-temperature record in subduction process: a Review of worldwide lawsonite eclogites: Lithos (in press).

Unger, L.S., Sisson, V.B., and Avé Lallemant, H.G., 2005, Tectonic setting of the Villa de Cura blueschists, Venezuela, based on major, minor, and trace elements, *in* Avé Lallemant, H.G., and Sisson, V.B., eds., Caribbean/South American plate interactions: Geological Society of America Special Paper 394, p. 233–249.

Usui, T., Nakamura, E., Kobayashi, K., and Maruyama, S., 2003, Fate of the subducted Farallon plate inferred from eclogite xenoliths in the Colorado Plateau: Geology, v. 31, p. 589–592, doi: 10.1130/0091-7613(2003)031<0589:FOTSFP>2.0.CO;2.

Watson, K.D., and Morton, D.M., 1969, Eclogite inclusions in kimberlite pipes at Garnet Ridge, northeastern Arizona: The American Mineralogist, v. 54, p. 267–285.

Yamasaki, T., and Seno, T., 2003. Double seismic zone and dehydration embrittlement of the subducting slab: Journal of Geophysical Research, v. 108, 2212, doi: 10.1029/2002JB001918.

Zack, T., Rivers, T., Brumm, R., and Kronz, A., 2004, Cold subduction of oceanic crust: Implications from a lawsonite eclogite from the Dominican Republic: European Journal of Mineralogy, v. 16, p. 909–916, doi: 10.1127/0935-1221/2004/0016-0909.

Zhang, H., Thurber, C.H., Shelly, D., Ide, S., Beroza, G.C., and Hasegawa, A., 2004, High-resolution subducting slab structure beneath northern Honshu, Japan, revealed by double-difference tomography: Geology, v. 32, p. 361–364, doi: 10.1130/G20261.2.

Manuscript Accepted by the Society 21 September 2005

Printed in the USA